AGU PUBLICATIONS

Global Biogeochemical Cycles

RESEARCH ARTICLE
10.1002/2015GB005349

Key Points:
- Net community production (NCP) was measured over 6 years with chemical sensors on six profiling floats
- NCP rates remained positive from middle winter to autumn
- Linking nitrate- and oxygen-based NCP rates allow gas exchange parameterizations to be optimized

Correspondence to:
J. N. Plant,
jplant@mbari.org

Citation:
Plant, J. N., K. S. Johnson, C. M. Sakamoto, H. W. Jannasch, L. J. Coletti, S. C. Riser, and D. D. Swift (2016), Net community production at Ocean Station Papa observed with nitrate and oxygen sensors on profiling floats, *Global Biogeochem. Cycles, 30*, 859–879, doi:10.1002/2015GB005349.

Received 4 DEC 2015
Accepted 30 MAY 2016
Accepted article online 1 JUN 2016
Published online 22 JUN 2016

Net community production at Ocean Station Papa observed with nitrate and oxygen sensors on profiling floats

Joshua N. Plant[1], Kenneth S. Johnson[1], Carole M. Sakamoto[1], Hans W. Jannasch[1], Luke J. Coletti[1], Stephen C. Riser[2], and Dana D. Swift[2]

[1]Monterey Bay Aquarium Research Institute, Moss Landing, California, USA, [2]School of Oceanography, University of Washington, Seattle, Washington, USA

Abstract Six profiling floats equipped with nitrate and oxygen sensors were deployed at Ocean Station P in the Gulf of Alaska. The resulting six calendar years and 10 float years of nitrate and oxygen data were used to determine an average annual cycle for net community production (NCP) in the top 35 m of the water column. NCP became positive in February as soon as the mixing activity in the surface layer began to weaken, but nearly 3 months before the traditionally defined mixed layer began to shoal from its winter time maximum. NCP displayed two maxima, one toward the end of May and another in August with a summertime minimum in June corresponding to the historical peak in mesozooplankton biomass. The average annual NCP was determined to be 1.5 ± 0.6 mol C m^{-2} yr^{-1} using nitrate and 1.5 ± 0.7 mol C m^{-2} yr^{-1} using oxygen. The results from oxygen data proved to be quite sensitive to the gas exchange model used as well as the accuracy of the oxygen measurement. Gas exchange models optimized for carbon dioxide flux generally ignore transport due to gas exchange through the injection of bubbles, and these models yield NCP values that are two to three time higher than the nitrate-based estimates. If nitrate and oxygen NCP rates are assumed to be related by the Redfield model, we show that the oxygen gas exchange model can be optimized by tuning the exchange terms to reproduce the nitrate NCP annual cycle.

1. Introduction

Net community production (NCP) is the balance between gross primary organic carbon production and all respiratory losses of organic carbon, including nitrification [*Laws*, 1991; *Williams*, 1993]. NCP is generally defined as a vertical integral down to a specified depth, often a depth near the base of the mixed layer or the euphotic zone. At a steady state, the annual net community production (ANCP) must be balanced by the export of an equivalent amount of organic carbon below this integration depth. This ANCP and associated export production (EP) is responsible for increasing dissolved inorganic carbon at depth, which in turn suppresses atmospheric carbon dioxide levels by 150–200 ppm by volume compared to an abiotic ocean [*Falkowski et al.*, 2000; *Watson and Orr*, 2003; *Parekh et al.*, 2006]. Despite the importance of NCP and EP in modulating atmospheric carbon dioxide levels [*Watson and Orr*, 2003], few open ocean measurements of ANCP exist due to the time and effort required to capture an annual cycle.

ANCP can be estimated by quantifying the annual biological production of oxygen or drawdown of nitrate within the mixed layer which can then be converted to a carbon estimate using Redfield stoichiometry. The limited measurements for ANCP that do exist have been determined at time series stations such as the Hawaii Ocean Time-series (HOT), Bermuda Atlantic Time-series Station (BATS), or Ocean Station Papa (OSP). Even these data sets can be biased toward nonwinter periods. Financial constraints make it unlikely that increases in data coverage will occur through new, ship-based time series stations. One solution is to use profiling floats to increase the density of NCP measurements.

Advances in sensor technology now allow profiling floats of the type used in the Argo array to be equipped with biogeochemical sensors [*Johnson et al.*, 2009]. Presently, about 250 floats are measuring oxygen [*Körtzinger et al.*, 2004; *Riser and Johnson*, 2008]. Some 70 of these are also measuring nitrate [*Johnson et al.*, 2010; *Johnson et al.*, 2013; *D'Ortenzio et al.*, 2014]. The floats equipped with biogeochemical sensors generally complete a profile from 1000–2000 m to the surface once every 5–10 days, typically collecting measurements at 60 depths during their assent [*Johnson et al.*, 2013]. Six profiling floats

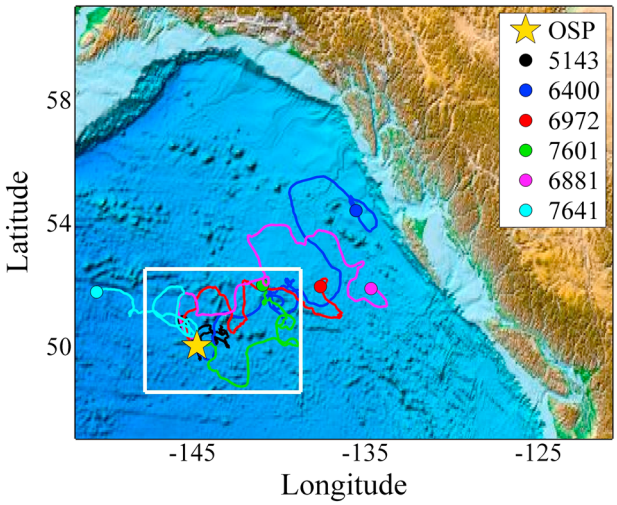

Figure 1. Float tracks for the six biogeochemical profiling floats deployed at OSP (gold star, 50°N and 145°W). Only data within the white rectangle (48.5N, 52.5N, −148W, −139W) were used in this study. Background topography is from ETOPO1 [*Amante and Eakins*, 2009].

equipped with nitrate and oxygen sensors have been deployed at OSP (Figure 1) in the Northeast Pacific. These floats have produced 10 complete float years of data over a period spanning six calendar years.

Here we examine the data set produced by these six floats near OSP. We find that the records of nitrate inventories in the water column enable robust estimates of ANCP. Additionally, these data provide insights into the seasonality, fate, and variability of the net organic carbon produced in the upper ocean. Estimates of ANCP using oxygen data are highly dependent on the gas exchange model used as well as small variations in sensor calibration. If it is accepted that oxygen and nitrate should cycle in nearly Redfield proportions, then the pattern of nitrate NCP can be used to place important constraints on air-sea exchange of oxygen.

2. OSP Background

OSP is located on the southeast edge of the Alaskan Gyre at 50°N and 145°W (Figure 1). Six years after its establishment as weather ship station P in 1943, routine bathythermograph profiles were included in the data collection. By 1956 the Line P hydrographic stations were initiated by the Pacific Oceanographic Group of the Fisheries Research Board of Canada. These stations set the stage for one of the longest continuing oceanographic time series which is now operated by Department of Fisheries and Ocean Canada's Institute of Ocean Sciences [*Freeland*, 2007]. Ocean Station Papa is now sampled by ship three times per year, in February, June, and August/September.

The seasonal variability of the surface mixed layer is well described by *Whitney and Freeland* [1999] and *Peña and Varela* [2007], but a short description derived from the biogeochemical float data follows. A permanent and sharp salinity gradient at ~120 m (halocline) creates a pronounced density gradient that limits mixing of the water column to this depth. This maximum mixing depth coincides roughly with the 33.1 isohaline on the practical salinity scale (pss). The deepest mixing occurs around February to March and entrains nitrate, salt, and iron back into the surface layer each year. Seasonally, the waters above the halocline begin to warm and freshen starting around April. This, in concert with decreasing wind speeds, causes the mixed layer to shoal to a minimum depth around 20 m by August. Here the mixed layer depth is defined as the depth at which the density first becomes 0.1 kg m^{-3} greater than the surface value. As soon as the mixed layer starts to shoal, the net production of organic matter promotes a drawdown of nitrate. By mid-September the surface waters lose about 7 μM of nitrate, but nitrate rarely becomes depleted in these high-nutrient, low-chlorophyll (HNLC) surface waters [*Peña and Varela*, 2007]. Iron and low wintertime light flux are thought to moderate phytoplankton growth and control the community composition of plankton which ultimately determines the recycling efficiency within the mixed layer and thus the amount of nutrient depletion and organic carbon exported below the halocline [*Miller et al.*, 1991; *Boyd et al.*, 1996; *Sunda and Huntsman*, 1997; *Maldonado et al.*, 1999]

3. Methods

3.1. Biogeochemical Profiling Floats

Six biogeochemical profiling floats were deployed at OSP between August 2008 and June 2013 and are identified by our float identification numbers as well as their World Meteorological Organization (WMO) numbers in Table 1. The float trajectories can be seen in Figure 1. The Teledyne/Webb Research Autonomous Profiling

Table 1. Float Information and Sensor Precision[a]

Float I.D.	WMO #	First Profile	Last Profile	Nitrate Sensor	NO3 1 SD (μM)	Oxygen Sensor	Oxygen 1 SD (μM)
5143	5902128	31 Aug 2008	10 Aug 2011	ISUS	0.15	3830	0.44
6400	5903274	18 Jun 2010	15 Jun 2014	ISUS	0.78	3830	0.54
6972	5903405	16 Feb 2011	17 Dec 2014	ISUS	0.17	3830	0.74
7601	5903714	16 Feb 2012	02 Dec 2015	ISUS	0.22	4330	0.34
6881	5903891	13 Feb 2013		ISUS	0.07	3830	0.44
7641	5904125	20 Jun 2013		SUNA	0.12	4330	0.22

[a]Precision was quantified by the standard deviation (SD) as calculated in section 4.1. The relative standard deviation for nitrate on float 6972 increased dramatically after 13 June 2013. Data after this point were not used in the calculation. Floats lacking a last profile date were still operating as of December 2015.

Explorer (APEX) floats were assembled at the University of Washington. Each float was augmented with an In Situ Ultraviolet Spectrophotometer (ISUS) optical nitrate sensor [*Johnson et al*., 2013] or the Submersible Nitrate UV Analyzer (SUNA) produced by Satlantic. Aanderaa model 3830 or 4330 optical oxygen sensors [*Tengberg et al*., 2006] were also mounted on each float. In addition, floats 6400 and 7601 were equipped with WetLabs FLBB optical chlorophyll fluorescence and backscatter sensors. The resolution of the 60 sampling depths increased as the floats ascended from their 1000 m park depth to their shallowest sample depth of 7 m (50 m resolution below 400 m, 5 m resolution above 100 m, and 10 m resolution in between). This approach better captured the higher variability in the surface waters. These APEX floats were designed to collect ~300 profiles, giving them a 4 year lifetime at their 5.25 day cycle interval. Data were retrieved from http://www.mbari.org/chemsensor/floatviz.htm which provides the quality controlled and adjusted data in near real time.

3.2. Sensor Calibration and Data Adjustment

3.2.1. Oxygen Data

Oxygen concentrations were computed using the manufacturer supplied calibration coefficients. These results tend to underestimate the actual oxygen concentration by 10 to 20% due to sensor drift while they are stored before deployment. However, once the sensors are deployed they do not appear to drift [*Tengberg et al*., 2006; *Bittig and Körtzinger*, 2015; *Johnson et al*., 2015]. We have recalibrated all of the oxygen sensors after deployment using a constant gain correction applied to the raw oxygen values ($O_{2,\,raw}$) for the entire data set for each float [*Johnson et al*., 2015].

$$O_{2,\,corr} = G \times O_{2,\,raw} \tag{1}$$

The sensor gain correction (G) for each float was determined by the surface saturation method described by *Takeshita et al*. [2013], except for float 7601. Float 7601 makes measurements of oxygen in the air while on the surface transmitting data, and the gain correction for this float was determined from these measurements [*Johnson et al*., 2015].

3.2.2. Nitrate Data

The nitrate sensor can undergo drift or offsets that occur as a constant concentration change over each profile [*Johnson et al*., 2013]. Drift and offsets in nitrate were determined by comparing the reported concentration at 1000 m depth to the gridded nitrate concentration reported in the World Ocean Atlas (WOA) 2009 [*Garcia et al*., 2010], after interpolation to the location of each profile. Long-term drift was determined from the slope of a linear regression of the difference in sensor nitrate and WOA nitrate versus time, and the offset was determined from the mean difference after correcting for drift. The accuracy of the calibrated oxygen and nitrate data is assessed by comparing the surface time series data to the values reported by the Line P program.

3.2.3. Optical Backscatter Data

The volume scattering function $\beta(\theta_C)$ with units of $m^{-1}\,sr^{-1}$ was calculated from the WetLabs FLBB sensor output using the manufacturer's equations and calibration coefficients with no further adjustments to the data. The backscatter coefficient due to particles (b_{bp}) was then estimated following the procedure of *Boss and Pegau* [2001]. Lastly, b_{bp} was used to compute particulate organic carbon (POC) using the linear regression equation $POC = 48811 \times b_{bp} - 24$, which is found in *Graff et al.* [2015].

3.3. Net Community Production Estimation

The net biological consumption of nitrate or production of oxygen can be used as a proxy for the net production of organic matter. However, the observed changes in nitrate and oxygen are produced by both physical and biological processes, and these need to be separated. Here a one-dimensional bulk mixed layer model, originally developed by *Price et al.* [1986], is used to simulate the mixed layer physical processes controlling nitrate and oxygen. Hereafter, the model will be referred to as PWP after the authors' initials. This model allows the biological component to then be separated from the physically driven change. The present implementation of PWP is a modification of the version developed by *Martz et al.* [2009] who in turn modified a version that was later published by *Glover et al.* [2011].

PWP was initially conceived to model the upper ocean's response to diurnal heating and wind-driven mixing over only a few days, but subsequent work has successfully extended the model run times from months to years [*Archer et al*., 1993; *Mathieu and deYoung*, 1995; *Babu et al*., 2004]. Float profile data were interpolated onto a model grid with 2 m vertical resolution. The PWP model was driven by the four times daily, atmospheric reanalysis data that are distributed by the National Centers for Environmental Prediction and the National Center for Atmospheric Research (NCEP/NCAR Reanalysis 1, *Kalnay et al.* [1996]). Data were extracted at the geographic location and time of each profile from: http://www.esrl.noaa.gov/psd/data/gridded/data.ncep.reanalysis.surfaceflux.html. At each time step in the model run (typically 90 min), the NCEP/NCAR Reanalysis 1 heat (latent, sensible, and radiation), freshwater (precipitation and evaporation), and momentum (wind) fluxes are applied to the model surface layer. Upwelling velocities were calculated from four times daily wind stress curl data obtained from the Environmental Research Division (ERD) of NOAA through their web site at http://las.pfeg.noaa.gov/thredds/dodsC/Model/FNMOC/. The curl was calculated by ERD from analyzed fields of sea level pressure from the Fleet Numerical Meteorology and Oceanography Center (http://www.usno.navy.mil/FNMOC). Ekman depth and vertical velocity attenuation were calculated following the approach of *Signorini et al.* [2001]. Oxygen was then exchanged across the top model layer. A variety of gas exchange models were tested, including those that incorporated gas transport through wave injected bubbles. These models will be described in more detail later.

Biological processes were not directly incorporated into the model. Instead, nitrate and oxygen concentrations (C) were treated as biologically inert tracers with the assumption that horizontal fluxes were small [*Chelton et al*., 2007; *Ren and Riser,* 2009] compared to changes driven locally by biology. The model was initialized with each float profile (F) at time n and run until the next profile time, $n+1$. The difference between the float data and the model results ($F-M$) were then determined at time $n+1$. This residual was attributed to biology, and a rate profile was calculated for each float time step. This rate profile was then converted to a carbon rate (NCP) using the modified Redfield stoichiometric ratio (R) for C:O (106:150) or C:N (106:−16) [*Anderson*, 1995]:

$$\left(\frac{\partial C}{\partial t}\right)_{\text{biology}} = \frac{\left(F_{t_{n+1}} - M_{t_{n+1}}\right)}{\left(t_{n+1} - t_n\right)} \times R \tag{2}$$

Unlike nitrate at OSP, oxygen in the mixed layer exchanges with the atmosphere. Equation (2) can account for the biological build up of oxygen in the water column, but it will neglect any oxygen that is biologically produced between t_{n+1} and t_n, and which escapes to the atmosphere. In the summer when the mixed layer is at it shallowest and oxygen supersaturation due to biology is at its highest, this missing atmospheric flux can be over 40% of the total biological oxygen production. Conversely enhanced respiration may increase the invasion of oxygen into the surface waters and dampen the actual respiration signal if only equation (2) were used. This additional biological production or loss of oxygen ($O2_{\text{bio}}$, mmol m^{-2}) can be approximated for each time step using equation (3):

$$O2_{bio} = \left(f_{net} - f_{phys}\right)\left(t_{n+1} - t_n\right) \tag{3}$$

where f_{net} is the net oxygen flux (mmol m^{-2} d^{-1}) and f_{phys} is the oxygen flux due to physics alone. The first calculated oxygen flux after the model is initialized with a float profile is used as an estimate for f_{net} since it includes the effects of both biology and physics. The last calculated flux prior to this initialization is used to estimate f_{phys}, since this is when the model ocean is driven closest to an abiotic state. $O2_{\text{bio}}$ can then be distributed over the mixed layer and added to F at time $n+1$ in equation (2) to calculate the NCP profile for oxygen.

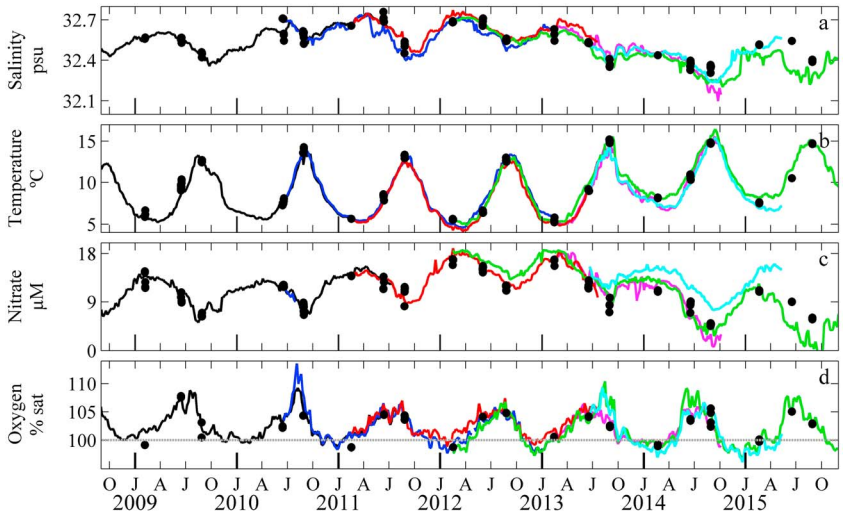

Figure 2. Average calibrated surface water properties measured by the profiling floats near OSP. Line P surface bottle data from stations at and near OSP (within the region defined by the white rectangle in Figure 1) are also plotted as filled black circles. Float numbers (and colors) are as follows: 5143 (black), 6972 (red), 7601 (green), 6881 (magenta), and 7641 (cyan).

The data sets often showed evidence of internal gravity waves that would cause vertical displacements in the water column between float profiles, displacement that the PWP model could not account for. This unmodeled physics would then show up as unrealistically high and temporally oscillating NCP rates around the mixed layer where small vertical displacement resulted in relatively large concentration differences between the float and model profiles. To correct for this, each model depth profile was adjusted before the rate profile was calculated from equation (2). Below the mixed layer, the model depth values were adjusted using density as a guide. For each model density measurement, a depth from the float profile was determined at an equal density. This depth then replaced the model depth at that density. Above the mixed layer the model depths were linearly expanded or contracted to meet the shallowest adjusted depth. Finally, all data sets were linearly interpolated back to the model depth grid using the adjusted depth profile.

4. Results

4.1. Float Data

The analytical precision of the nitrate and oxygen sensors were assessed by measuring their variability in the surface mixed layer, which was assumed to be well mixed with respect to oxygen and nitrate. The standard deviation of the shallowest 3 to 5 samples above the mixed layer depth was calculated for each profile, and then the average for each float was reported in Table 1. If the mixed layer depth was greater than 27 m, all five samples could be used. Except for float 6400, the average standard deviation for nitrate was less than 0.22 µM. The 3.5 times higher standard deviation observed for float 6400 resulted from very low light throughput in the nitrate sensor. The sensor optics may have been damaged during transit or deployment. The average oxygen precision was better than 0.74 µM for all floats.

The average surface values for the calibrated float data were determined using the same surface mixed layer criteria described above. In Figure 2, these average values are compared directly to contemporaneous discrete observations shallower than 20 m collected by the Line P Program at or near OSP. Line P data were provided by the Ocean Sciences Division from the Pacific Region of the Institute of Ocean Sciences Data, Fisheries and Oceans Canada. Surface float data were interpolated to the timestamp of the Line P observations. The quality-controlled float nitrate and oxygen concentrations in Figures 2c and 2d closely match the bottle data results. Average differences (±1 standard deviation error limits) from the Line P Program data for nitrate, percent oxygen saturation, salinity, and temperature were -0.61 ± 1.8 µM, -0.64 ± 1.4%, 0.02 ± 0.05 pss, and 0.13 ± 0.58°C, respectively. These differences are much smaller than the amplitude of the seasonal cycles. The variability in differences observed for all properties is probably reflective of small changes in water mass properties as the floats move further from OSP.

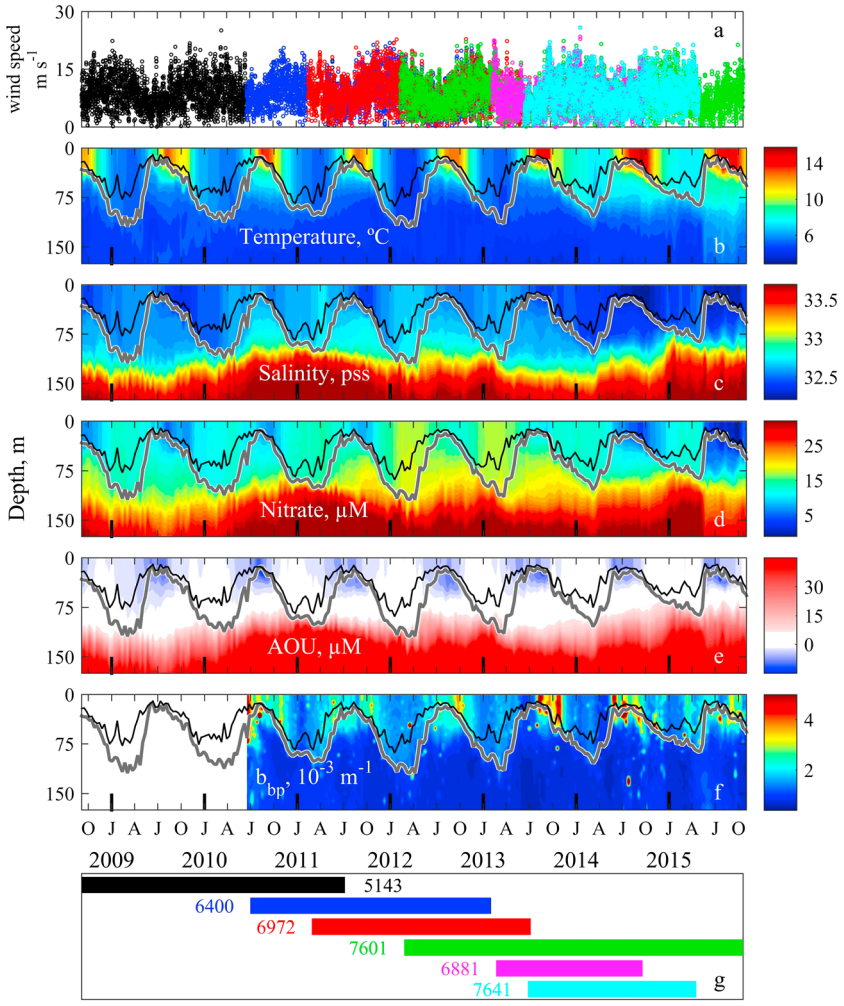

Figure 3. (a) NCEP wind speeds along the float tracks, (b–f) water properties observed by the profiling floats above the halocline, and (g) float deployment durations within the bounding box shown in Figure 1. Thick grey lines represent the mixed layer depth (depth of 0.1 kg m^{-3} density difference from the surface value). Thin black lines define the average mixing depths determined by the model. Colors in 4a match those in 4g. *X* axis tick labels represent the repeated months: January, April, July, and October.

The seasonal cycles observed by the profiling floats for temperature, salinity, nitrate, oxygen, and the particle backscatter coefficient (b_{bp}) are shown in Figure 3 and as time/depth contour plots. Superimposed upon the contour plots are the mixed layer depth in grey and the model mixing depth in black. The model mixing depth is the average depth the model mixes to between float surfacing. Each spring and summer, as the surface waters warm and freshen, there is a distinct loss of nitrate from the mixed layer implying a net production of organic matter that incorporates fixed nitrogen. The decrease measured by the floats is consistent with the nitrate annual cycles observed during the weather ship era at OSP [*Wong et al.*, 1998].

There is significant interannual variability in the maximum nitrate concentration reached in the surface waters during winter (19.2 to 13.9 µM, Figure 2c). The highest nitrate concentrations occur in winters with the lowest surface water temperature. In part, this may reflect deeper mixing that brings colder, saltier, and more nutrient-rich water to the surface. But the signal is also driven by longer-term vertical displacements and gradient changes in the halocline that can enhance or limit entrainment during deep winter mixing. For example, Figure 3c shows up to 70 m changes in the depth of the 33.1 (pss) isohaline as well as changes in the concentration gradients of nitrate and oxygen (Figures 3d and 3e) at this depth. Figures 2b and 3b also show that the surface waters near OSP are around 2° warmer than the previous 5 years, beginning in the summer of 2013. This is consistent with broader scale patterns recently observed in the

northeast pacific [*Bond et al*., 2015]. The divergence in nitrate values seen in Figure 2c (and salinity and temperature to some extent, Figures 2a and 2b) between floats 7601 (green) and 7641 (cyan) starting in 2014 reflects the motion of the floats away from Station P. Float 7601 moves northeast away from the HNLC region and into warmer, fresher, and more nitrate depleted waters. Unlike all other floats 7641 has moved northwest into the heart of the HNLC region of the gyre (see Figure 1). The values of nitrate observed by these floats bracket the nitrate measured at Station P during the summer of 2014.

The annual oscillations in oxygen concentration and saturation within the mixed layer at OSP are dominated by temperature-induced changes in oxygen solubility [*Emerson and Stump*, 2010]. As the water warms in spring and summer, decreasing solubility causes evasion of oxygen to the atmosphere. In the mixed layer oxygen tends to equilibrate with the atmosphere in a few weeks to a month [*Broecker and Peng*, 1974; *Luz and Barkan*, 2000]. This small lag in equilibration time produces supersaturation with respect to oxygen as the ocean warms (Figure 2d). In contrast to the supersaturation resulting from the warming mixed layer, bubble injection may cause supersaturation at any time of the year, but especially in winter when the wind speeds are at their greatest. Finally, biological production may also drive saturation changes, but this is often the smallest of the three processes impacting percent saturation, except during late spring and summer [*Emerson and Stump*, 2010]. In Figure 3e, oxygen is plotted as apparent oxygen utilization (AOU) to emphasize the concentration changes relative to 100% saturation state. AOU is the difference between the expected saturation concentration and the observed concentration. Waters directly below the winter mixed layer depth do not have annual contact with the atmosphere and have become depleted in oxygen by around 40 μM due to respiration of organic matter, while the negative AOU values during the summer reflect the biological production of oxygen in the mixed layer. In Figure 2d, oxygen is plotted as percent saturation to emphasize that oxygen is supersaturated in surface waters for a majority of the season. Physical processes can supersaturate the surface water up to a few percent, values above that tend to be due to net primary production [*Woolf and Thorpe*, 1991; *Emerson et al*., 1991].

In addition to the chemical measurements shown in Figures 2 and 3, floats 6400 and 7601 were equipped with biooptical sensors for chlorophyll fluorescence and particle backscatter. The chlorophyll fluorescence data are not utilized in this study, but the particle backscattering coefficient is used to estimate particulate organic carbon. Figure 3f shows the particulate backscattering coefficient measured by these floats above the 33.1 (pss) isohaline. Each summer and fall there is a distinct increase in particles that tends to coincide with the drawdown of nitrate (compare Figures 3d and 3f). But it is also interesting to note that minima in optical backscatter can occur in summer as well as in winter. For example, there is a strong minimum in January of 2011 when the winter mixed layer is near 100 m, but the waters are also optically clear in July 2013 when the mixed layer is shallow and nitrate has been drawn down to some extent.

4.2. Model Optimization

The overarching goal of our work is to use changes in the nitrate and oxygen inventories through time in conjunction with a physical model to estimate ANCP as well as the seasonal evolution of NCP and its ultimate fate in the water column. Before these estimates were calculated, the PWP model was tuned to the local conditions at OSP so that the physical processes could be accurately represented and isolated from the biological processes. There are three tunable parameters: a vertical eddy diffusion coefficient and offsets for the net heat and freshwater fluxes. The latter two parameters account for fluxes of heat and salt that the one-dimensional model cannot represent. These may be horizontal fluxes, uncertainty in the derived surface fluxes of heat and fresh water obtained from atmospheric reanalysis data set as well as any potential model-induced artifacts. Mixing due to diffusion is most important below the mixed layer since surface forcing in the model homogenizes the mixed layer first and any diffusional mixing requires a gradient in depth for the property being mixed. Here an eddy diffusion coefficient of $1.5 \times 10^{-5}\,m^2\,s^{-1}$ was used. This is the average value determined by *Matear and Wong* [1997] for the base of the mixed layer near OSP. This value is also very similar to the value of $1.0 \times 10^{-5}\,m^2\,s^{-1}$ used by *Emerson and Stump* [2010] at OSP. No additional tuning of the eddy diffusion coefficient was attempted.

The capability of a 1-D model to reproduce the physical processes was assessed by initializing the model with the first float profile and then allowing the model to run forward with only the NCEP fluxes to constrain the calculations. Figure 4 shows the optimized model results over 3 years for float 5143 when $23\,W\,m^{-2}$ of heat and $0.3\,m\,yr^{-1}$ ($9.5\,mg\,m^{-2}\,s^{-1}$) of freshwater were continuously removed from the model ocean surface, in

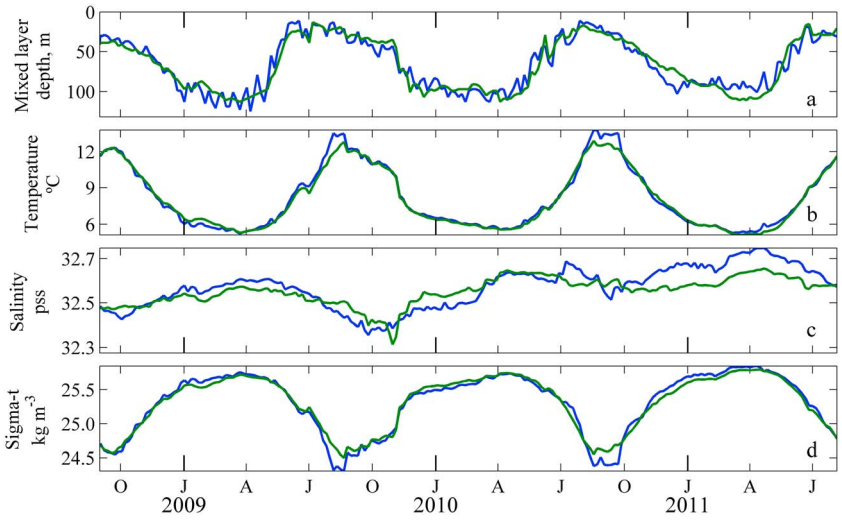

Figure 4. Optimized model results (green) compared to profile data from float 5143 (blue) (average of top 30 m). Model was initialized with profile number 1 and run out 3 years with no relaxation to the observations. *X* axis tick labels are identical to Figure 3 above.

addition to the time varying fluxes obtained from the NCEP reanalysis data set. The model surface temperature, salinity, density, and mixed layer depth agree quite well with the float data even after almost 3 years. It is important to remember that the model was only initialized once. No other adjustment was needed to bring the model back in line with the float data.

The model does not warm the surface layer quite enough when the mixed layer reaches its shallowest depth in summer (Figure 4b). There are several possible explanations for this. We use a constant heat offset value to close the heat budget. In reality there may be some seasonal variability to this term [*Large*, 1996]. Second, the NCEP reanalysis climate data used to force the model may have inaccuracies in the data set. Yet another possibility is that higher biomass in summer could lead to a shallower light penetration depth, trapping heat to a shallower depth. When the mixed layer is at its shallowest, it is most responsive to changes in atmospheric forcing. When the actual rates are determined though, the model is reinitialized at every profile and model float differences rarely exceed 0.5° which has the potential to underestimate summertime NCP by 12% and ANCP by 4%. Except for upwelling and diffusion, the PWP model is forced at the surface and has no means to accommodate changes in water column structure due to forcing from below. Despite this limitation, PWP realistically creates seasonal changes in the mixed layer and surface density suggesting the major physical processes are adequately captured.

The offsets in heat and freshwater inputs are consistent with observations of horizontal flow not accounted for by the model. *Ren and Riser* [2009] calculate an average geostrophic velocity for waters near OSP of about 2.5 km/d toward the northeast with little seasonal variability. This flow imports saltier water from the southwest that is equivalent to a salinity increase of 0.17 pss over the course of the year. This salinity tendency counters that from Ekman advection that brings fresher water to the region from the north. The net result is about a 0.09 pss yr^{-1} increase in salinity near OSP. This is equivalent to removing about 0.15 m yr^{-1} given an average mixed layer salinity of 32.5 pss and an average mixed layer depth of 61 m (the averages for all floats).

Our tuning offset removes 0.3 m yr^{-1} to close the salt budget which is within 1 standard deviation of the salinity tendency measured by *Ren and Riser* [2009]. It is also interesting to note that the 23 W m^{-2} of heat that needs to be removed from the PWP model closely matches the average imbalance estimated for OSP by *Large* [1996] of 25 W m^{-2}. These lines of evidence suggest the tuning parameters may be accounting for horizontal advection of salt and heat from geostrophic flow that the one-dimensional model cannot account for. Another possibility recently suggested by *Freeland* [2013] is that enhanced upward advection of cold salty water, not accounted for by the model, could also contribute to these heat and salt imbalances.

4.3. Model Oxygen Flux

In our rate calculations, oxygen is transferred across the top model layer using the approach outlined by *Stanley et al.* [2009] and *Liang et al.* [2013], where the net oxygen flux, F_T, (mol m^{-2} s^{-1}) is the sum of diffusive gas exchange (F_{EX}) and the injection of oxygen into the surface waters via completely (F_C) and partially (F_P) dissolving bubbles

$$F_T = F_{EX} + F_C + F_P. \quad (4)$$

However, the NCP rates determined from oxygen data are highly dependent upon the formulation of the gas transfer model so a variety of models were tested. Five gas exchange models with either quadratic [*Wanninkhof*, 1992; *Wanninkhof*, 2014] or cubic [*McGillis et al.*, 2001; *Prytherch et al.*, 2010; *Ho et al.*, 2011] dependencies of F_{EX} on wind speed, but no bubble transport terms ($F_C = 0$, $F_P = 0$) were tested. These models have been primarily tuned to reproduce the flux of carbon dioxide, which is less sensitive to bubble transport due to the high solubility of carbon dioxide. Three formulations that included the bubble transport of gas were also tested [*Woolf and Thorpe*, 1991; *Stanley et al.*, 2009; *Liang et al.*, 2013]. *Stanley et al.* [2009] use an inverse approach constrained by 3 years of noble gas measurements at BATS to partition the fluxes on the right hand side of equation (3), while *Woolf and Thorpe* [1991] and *Liang et al.* [2013] estimate the bubble fluxes directly from modeled populations of subsurface bubbles. *Woolf and Thorpe* [1991] condense the bubble flux terms to a quadratic function of wind speed which increases the equilibrium saturation state of the ocean as wind speeds increase. The gas flux is then treated as purely diffusive ($F_C = 0$, $F_P = 0$).

The *Liang et al.* [2013] model is somewhat unique when compared to the other models. The gas flux from bubble injection is truly separated from the diffusive gas exchange, and the fluxes are related to the friction velocity instead of wind speed. The authors then use modeled bubble populations, which are simulated with a physically realistic model in the turbulent boundary layer of the surface ocean, versus friction velocity to constrain these gas fluxes. We focus much of our discussion on this model since it is a recent and comprehensive synthesis and it is applicable to a variety of gases.

Despite the detail of work in *Liang et al.* [2013] there are still uncertainties in gas flux estimates. In addition to evaluating published gas exchange models, two models (*Liang et al.* [2013] and *Stanley et al.* [2009]) were optimized by tuning the various transport terms to produce an oxygen-based annual NCP cycle that best matched the annual mean cycle of NCP determined from nitrate in a least squares sense. It was assumed that nitrate and oxygen could be related by Redfield stoichiometry. The results of this optimization procedure are discussed in section (4.4).

4.4. NCP at OSP

Net community production rates were calculated using nitrate and oxygen data from five of the six floats deployed at OSP. Float 6400 data were excluded from nitrate and oxygen-based NCP calculations due to the lower quality of the nitrate data it returned. Only data collected from profiles within the white box in Figure 1 were used for rate calculations. This allowed a continuous temporal data record and minimized the influence of the Alaskan Current waters on rate calculations from some of the most northeasterly portions of the float trajectories for floats 6972 and 6881. This subset of the data included over six calendar years of data from 2009 to 2014 and over 10 complete float years of data.

4.4.1. Average Seasonal NCP Calculation

All floats completed a profile every 5.25 days, which yielded a NCP rate profile derived from nitrate and oxygen for each interval. To create an average seasonal NCP cycle using the 10 float years of data, each calendar year was broken into identical 7 day bins. The rate profiles for each float were then averaged into these bins. This choice was arbitrary, but it allowed for high resolution while at the same time assuring that each bin was populated with data for a given time series. When multiple floats were profiling in the same year, identical bins were averaged to produce a single rate profile for that bin in a given year. This was done to avoid biases from multiple floats in a year where anomalous properties from one float might add too much weight to such a year. This assumes that the difference between floats for a given year represented methodological variability and not true differences in NCP. Finally, the six calendar years were averaged to yield a mean rate profile for each weekly bin in the “average year". Integration of these profiles down to a chosen depth yields an estimate for the average seasonal NCP cycle for the region within the white box in Figure 1.

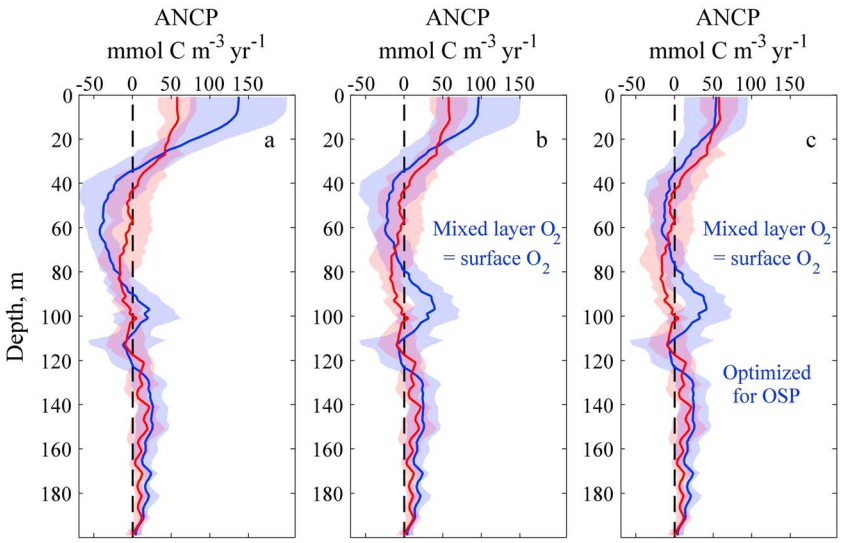

Figure 5. Average vertical profiles of ANCP for 2009–2014. (a) ANCP determined from nitrate inventories in red and from oxygen inventories in blue using all sensor data. (b) Same as in Figure 5a but the mixed layer oxygen concentrations for the months of October through April were set to the mean of the two shallowest values on the profile before NCP rates were calculated. (c) Same as in Figure 5b but *Liang et al.* [2013] gas flux model was tuned for OSP.

4.4.2. Average ANCP Calculation

ANCP is then determined by integrating the weekly binned profiles over the course of the average year. This can be reported as a vertical profile (mmol C m^{-3} yr^{-1}) or as a single value when integrated to a specified depth (mmol C m^{-2} yr^{-1}). For the latter approach, ANCP is also reported for each float year when a float contains data spanning a complete year starting on 1 January. This approach uses less of the float data, as it excludes less than complete calendar years for any float, but allows a comparison between individual floats and years.

Figure 5 shows the annual mean vertical profiles of nitrate- and oxygen-derived ANCP determined from the 1-D model using data from all years. The oxygen ANCP rates in Figure 5 were calculated using the *Liang et al.* [2013] gas exchange model. The 95% confidence intervals based on the standard deviation of the six calendar years of data are shown as the shaded regions about each ANCP profile.

In Figure 5a, vertical rate profiles of ANCP computed with all nitrate and oxygen data are shown. Both profiles in Figure 5a exhibit positive ANCP in the top 30 m, both profiles taper to zero between 30 and 40 m, and both estimates show negative rates in the 30 m to 100 m range. However, the amplitude of the oxygen-based rate is 2.5 times greater than the nitrate-based rate in the surface 30 m and up to 2 times greater in the 30 m to 100 m zone. Additionally, the confidence intervals barely overlap in the top 30 m. Below about 120 m both rates are slightly positive. This depth is below the depth of winter mixing as well as base the euphotic zone [*Sherry et al.*, 1999; *Harrison et al.*, 2004]. It is unlikely that this positive NCP measured at depth is a true biological signal and more likely to be a result of physical processes such as the temporal change in deep nitrate concentrations that are not captured by the model. The positive peak in ANCP around 100 m is especially prominent in the oxygen-based estimate. This is a depth range with rapid changes in oxygen. It coincides with the depth of deep winter mixing and is also below the euphotic zone depth. Again, it is unlikely that biological processes are producing oxygen in this region, so we attribute this peak to model inaccuracies and focus on the data above 80 m.

4.4.3. Oxygen ANCP Amplitude

The positive and negative ANCP rates computed with all oxygen data in the upper 90 m are larger than those of nitrate. This may be an artifact of the slow response rate of the oxygen sensor [*Bittig et al.*, 2014]. During periods of deep mixing the vertical oxygen gradient is quite steep below the base of the mixed layer (Figure 6). As the float ascends into the mixed layer the reported oxygen values may be several micromolar low as the oxygen sensor continues to equilibrate with the higher oxygen concentrations encountered in the well-mixed surface layer. This slow response can be seen in Figure 6, where the temperature profile is

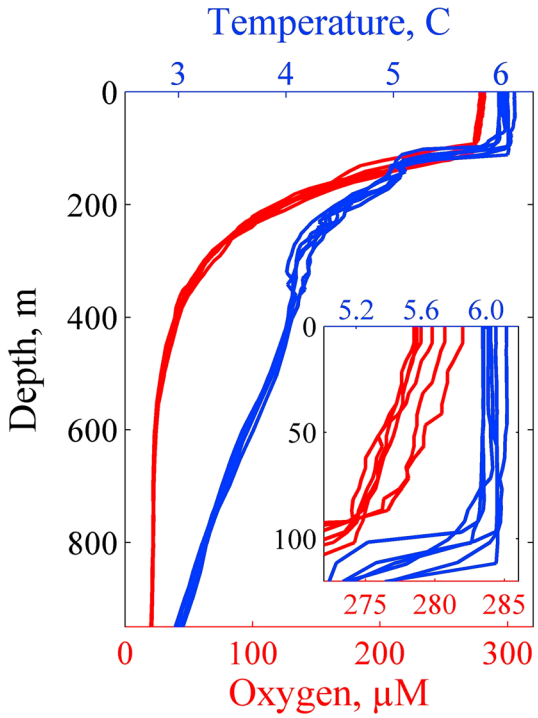

Figure 6. Vertical profiles of oxygen and temperature during February 2010 reported by float 5143. Inset shows the upper 120 m.

vertically uniform in the well-mixed layer while the oxygen profile shows a 5 µM linear increase over the same range (~1.8% change).

If the low values of oxygen near the bottom of the mixed layer result from a slow sensor response, then this effect appears as an enhanced oxygen consumption rate. If the model is initialized with the slightly low oxygen values observed by the float, vertical mixing and air-sea exchange in the model will increase oxygen values in this depth range. At the time of the next profile the float oxygen concentrations are lower than those of the model. This results in an apparent biological loss of oxygen (oxygen consumption) and a negative NCP rate (equation (2)).

At the same time though this vertical mixing due to this concentration discrepancy actually decreases the model surface oxygen concentration slightly (<1%) compared to the float profile. In the winter when mixing is deep, oxygen equilibration with the atmosphere can take a month. The end result is that the model never quite equilibrates with the atmosphere before the next float profile time, and this appears as enhanced positive NCP in the shallow surface waters (equation (2)). The combined result is enhanced negative ANCP in the 40 m to 90 m depth range and enhanced positive ANCP in the top 40 m or so.

The artifact in rates from a slow oxygen sensor response rapidly decays as the float rises through waters with more uniform oxygen concentrations and the sensor catches up to ambient values. Calculations of NCP rates could be corrected by either adding artificial lags to the oxygen sensor data or the effect can by assessed by setting all oxygen concentrations in the mixed layer to the mean of the two shallowest surface values during months when deep mixing occurs. This latter change presumes that mixed layer oxygen should be homogeneous and the best estimate of the concentration comes from the shallowest values. Such changes, when implemented in the model, decrease both the large negative and positive ANCP in the top 90 m of the water, though the variations are still greater than those seen in the nitrate-based ANCP profile (Figure 5b). However, above 90 m, the average ANCP profiles based on nitrate and oxygen measurements are now more consistent. We believe the greater swings in oxygen-based ANCP rates observed in Figure 5a are an artifact of the sensor response. Since the oxygen-based estimates appear to be very sensitive to the accuracy of the oxygen measurements we consider the nitrate-based ANCP rates most definitive. Further discussion of oxygen-based NCP and ANCP estimates will rely on this adjusted oxygen data set. We note that errors due to this artifact are maximal in the north Pacific, because well-oxygenated surface waters overlie a very strong oxygen minimum.

4.4.4. NCP Seasonal Cycle

To compute integrated NCP values, we chose integration depths of 35 and 80 m for both nitrate and oxygen. The vertical ANCP rates for both nitrate and oxygen first approach zero around 35 m and then remain less than zero down to 80 m (Figure 5). This implies that the annual net production of organic matter must occur above this depth. The mean oxygen rate crosses zero at 33 m, while the mean nitrate rates crosses zero at 43 m.

When the mixed layer begins to shoal in spring, it is possible to have net production of organic matter deeper than 35 m at OSP. Therefore, rates were also integrated down to 80 m which is deeper than either the deepest average model mixing depth or the euphotic zone at OSP. The PWP model assumes type IA waters [*Paulson and Simpson*, 1977], which yields a 1% of surface irradiance depth of 73 m, which is typically assumed to correspond to the euphotic zone depth. Direct measurements of the euphotic zone depth at OSP give a range between 30 and 80 m [*Sherry et al.*, 1999; *Harrison et al.*, 2004].

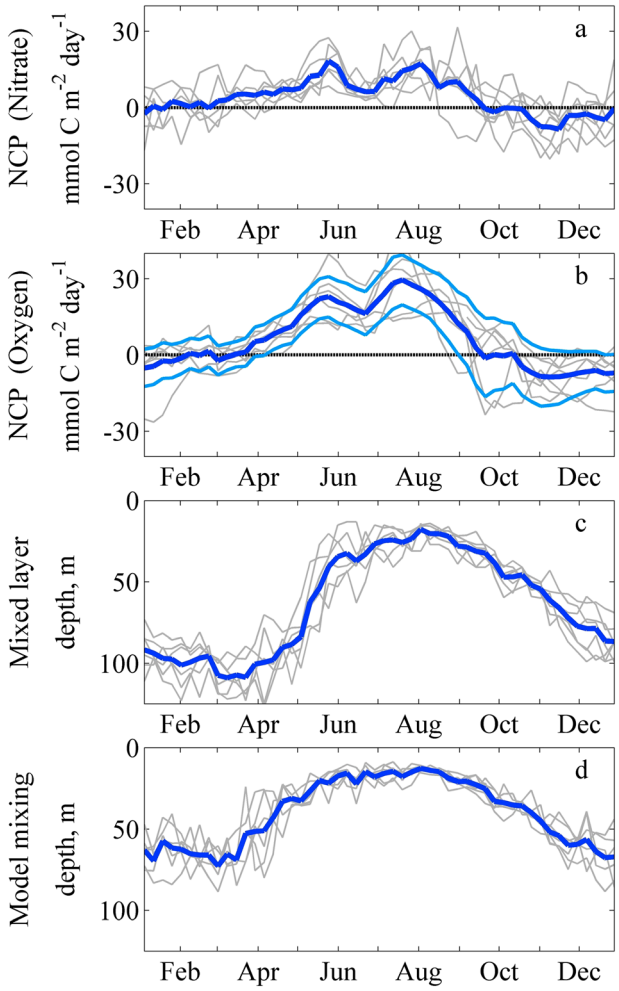

Figure 7. The average seasonal cycle for NCP calculated using (a) nitrate and (b) oxygen inventories integrated to 35 m, (c) the mixed layer depth, and (d) the average model mixing depth. The dark blue lines represent the average of all years and the grey lines are the individual years. The light blue lines in Figure 7b are the NCP cycles when oxygen concentrations in all float data sets are increased or decreased by 1% compared to the calibrated values. The average annual cycle for the mixed layer depth and model mixing depth were calculated in a similar manner to the NCP cycle.

Our results show that the deeper integration depth yields slightly lower ANCP estimates than the shallower estimates (data reported later) which would be expected as respiration becomes more important with depth, but the seasonal shape of the annual NCP cycle changes little. Therefore, the annual cycle data will be reported using the 35 m integrated results. Figures 7a and 7b show the average annual cycle of depth integrated NCP determined from nitrate and oxygen, respectively. Figure 7c shows the mixed layer depth, while Figure 7d shows the average depth over which mixing homogenized the upper ocean in the numerical model. NCP is positive from the beginning of February through mid-September (Figures 7a and 7b). The mixed layer does not begin to shoal appreciably until late April, nearly 3 months later than the onset of positive NCP. The shoaling of the model-based mixing depth shown in Figure 7d, which begins to decrease in mid-March, is more closely correlated to the time at which NCP becomes positive.

The mixed layer appears to shoal in two steps: from mid-April to mid-May the rate is 1.3 m d^{-1}, and from mid-May to mid-August the rate decreases to 0.24 m d^{-1}. A local maximum in nitrate-based NCP of 18.2 mmol C m^{-2} d^{-1} (95% confidence interval (CI) [10.9, 25.6]) occurs near the date at which mixing depth stabilizes near 20 m. A second NCP maximum of 17.2 mmol C m^{-2} d^{-1} (95% CI [11.0, 23.4]) occurs in August, just before the mixed layer starts to deepen again. The local NCP minimum between these two rate peaks drops to 6.3 mmol C m^{-2} d^{-1} (95% CI [2.7, 9.8]). Oxygen-based NCP exhibits similar patterns with slightly greater amplitude in the NCP signal, though the minimum is not significantly different than the maximum rates. By mid-September to mid October, NCP becomes negative implying a net respiration of organic matter through the end of December and into January as oxygen is utilized to oxidize organic nitrogen to nitrate. The stocks of particulate nitrogen in the mixed layer are generally too low to supply sufficient nitrate to support the presumed remineralization [*Varela and Harrison*, 1999]. Possibly dissolved organic nitrogen is consumed or the negative NCP rates result from unmodeled physics that brings low-oxygen, high-nitrate water into the mixed layer at rates higher than predicted by the PWP model.

The average ANCP determined from nitrate inventories is 1.5 mol C m^{-2} yr^{-1} (95% CI [0.9, 2.2]) while the rates for individual floats in any 1 year range between 0.8 and 3.1 mol C m^{-2} yr^{-1} from 2009 to 2014 (Table 2). For oxygen-based estimates, the average ANCP was 2.4 mol C m^{-2} yr^{-1} (95% CI [1.3, 3.5]), but the annual estimates from the floats in Table 2 varied from 0.1 to 3.8 mol C m^{-2} yr^{-1}. The range of the individual estimates of ANCP from oxygen is about what would be expected for ±1% errors in calibration of an oxygen sensor (Figure 7b). Although absolute accuracy is not required for rates derived from nitrate, as they are for oxygen

Table 2. Profiling Float ANCP Estimates[a]

		Annual net community production (moles C m^{-2} yr^{-1})						Average	SD
Proxy	Float	2009	2010	2011	2012	2013	2014	(Of All Years)	
Nitrate integrated to 35 m	5143	1.7	0.8						
	6972			1.5	1.2				
	7601				0.9	2.2	1.7		
	6881					3.1			
	7641						1.3		
Yearly average		1.7	0.8	1.5	1.0	2.6	1.5	1.5	0.6
Oxygen integrated to 35 m	5143	3.4	2.7						
	6972			3.8	3.5				
	7601				0.1	0.1	2.6		
	6881					0.3			
	7641						0.1		
Yearly average		3.4	2.7	3.8	1.8	0.2	1.3	2.2	1.4

[a]Rates were calculated for years with data coverage greater than 84%. Oxygen rates were calculates using the *Liang et al.* [2013] gas exchange model.

which is strongly influenced by gas exchange, the computed nitrate rates can be more biased by horizontal concentration gradients in the nitrate climatology. For example, if the nitrate climatology decreases along the direction of a float track, this decrease would not be accounted for in the physical model and would show up as enhanced NCP. Excluding data from profiles outside of the white rectangle in Figure 1 minimized this problem. Thus, there are advantages and disadvantages to the use of both sensors to determine ANCP. There is generally not enough data in any single year to assess whether different years have different rates.

4.5. Gas Exchange Model Optimization

The ANCP rates determined from oxygen concentrations with various gas exchange models show large differences (Figure 8). In particular, models that do not include bubble injection terms produce ANCP values

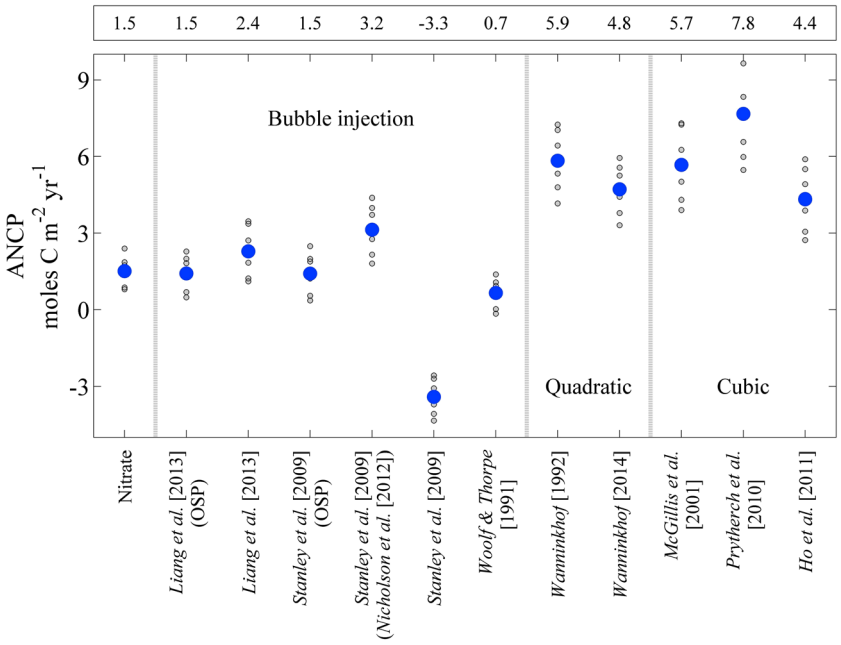

Figure 8. Model-derived estimates of ANCP for all years integrated to 35 m depth. Estimates based on nitrate measurements are compared to oxygen-based estimates using various gas flux parameterizations grouped by model type. Individual years are grey. Average of all years are blue and in the top row of values. Parentheses indicate different tunings for the *Liang et al.* [2013] or *Stanley et al.* [2009] formulations in this work (OSP) and by *Nicholson et al.* [2012]. Mean values include all data, not just complete calendar years, and are slightly different than found in Table 2.

that are systematically about 2 times higher than the mean of models that include bubble injection. A quadratic or cubic wind speed dependency has little impact on ANCP in the models that do not include bubble injection. These models were generally developed for carbon dioxide transport, which is less sensitive to bubble injection of gases due to the high solubility of carbon dioxide.

Unlike diffusive gas exchange, which can be either into or out of the ocean based on the air-sea concentration gradient, the bubble flux terms mainly enhance gas flux into the surface ocean. These bubble flux terms are necessary as previous observations [*Emerson et al.*, 1991; *Hamme and Emerson*, 2002; *Emerson and Stump*, 2010] indicate that inert gases are often significantly supersaturated near OSP and other locations due to wave injection of bubbles. This is especially important in fall and winter when the mixed layer cools and deepens as the wind speeds increase. In such conditions, where the water is cooling, the diffusive gas exchange component cannot produce gas supersaturation. There would be no physical means to supersaturate the surface waters during this period without bubble injection included in the model. Our rate computations using models with no bubble injection must substitute biological production of oxygen for bubble injection to produce the observed supersaturation of oxygen. This creates an artificially high ANCP. As a result, gas exchange models without bubble injection are not considered further in this paper.

The *Liang et al.* [2013] and *Woolf and Thorpe* [1991] bubble injection models produced ANCP rates (Figure 8) and NCP annual cycles that are reasonably consistent with the nitrate results when rates are scaled to carbon units by the Redfield ratio (Figures 7a and 7b). When the *Stanley et al.* [2009] formulation was tested, the average ANCP using the oxygen inventories observed by the float array was $-3.3\ \mathrm{mol\,C\,m^{-2}\,yr^{-1}}$. This negative rate is unrealistic and suggests that the surface ocean is net heterotrophic. It is not consistent with the nitrate ANCP estimate or with previous estimates by other researchers using oxygen [e.g., *Emerson and Stump* [2010]. The negative ANCP estimate is a result of the Stanley parameterization for complete bubble injection (F_C) producing a high influx of oxygen into the mixed layer at OSP. The oxygen concentration measured by the float is low in comparison to the concentration produced by the modeled bubble flux. Equation (2) then results in apparent oxygen consumption, and a negative NCP rate when the measured oxygen is lower than the modeled value.

Nicholson et al. [2012] used a version of the *Stanley et al.* [2009] model that was retuned at HOT and BATS to estimate gross primary production via triple oxygen isotope measurements. Their retuning reduced the importance of bubble fluxes by about 75%. As a result, when the *Nicholson et al.* [2012] gas exchange model is applied to the float data, the derived ANCP increases greatly, relative to the value computed with the *Stanley et al.* [2009] version. The Nicholson version produces ANCP rates that are about 1.5 times higher than the mean of the nitrate ANCP and the oxygen ANCP estimated using the *Liang et al.* [2013] model (Figure 8). The variability in ANCP with the two versions of the Stanley model suggests that one application of the float data would be to assess gas exchange rates by tuning an oxygen model to reproduce the NCP rates based on nitrate data.

The parameterizations in equation (4) for F_{EX}, F_C, and F_P that were used in *Stanley et al.* [2009] are shown in equations 5–7 below. At wind speeds less than $2.27\ \mathrm{m\,s^{-1}}$ the bubble fluxes are set to zero. All of the tunable parameters optimized in *Stanley et al.* [2009] are treated as constants, and an additional dimensionless multiplier, *G*, has been included in equations 5–7 for model optimization purposes. This allows much easier comparison to the *Stanley et al.* [2009] results since their tuning parameters also combine other constants, including those for white cap coverage and the air entrainment velocity. This approach is similar to the original approach used by *Stanley et al.* [2006] but uses the *Stanley et al.* [2009] results as a baseline.

$$F_{EX} = G_{EX}\cdot 0.97 \cdot 8.6 \times 10^{-7}\left(\frac{Sc}{660}\right)^{-0.5} u_{10}^{2}\left(C_{eq} - C_w\right) \tag{5}$$

$$F_C = G_C\cdot 9.1\times 10^{-11}\ \left(u_{10} - 2.27\right)^3 \frac{P_a}{RT} \tag{6}$$

$$F_P = G_P\cdot 2.3\times 10^{-3}\ \left(u_{10} - 2.27\right)^3 \alpha\left(\frac{D}{D_o}\right)^{\frac{2}{3}} \frac{\left(P_b - P_w\right)}{RT} \tag{7}$$

Diffusive gas exchange, F_{EX}, uses the gas transfer velocity formulated by *Wanninkhof* [1992]. The quadratic coefficient, 8.6×10^{-7}, has been converted to $\mathrm{s\,m^{-1}}$ and 0.97, formally a dimensionless tuning parameter added by *Stanley et al.* [2009], is now a dimensionless constant. *Sc* is the Schmidt number for oxygen

Table 3. *Stanley et al.* [2009] Model Tuning Coefficients

Reference	G_{EX}	G_C	G_P
Stanley et al. [2009]	1	1	1
Nicholson et al. [2012]	0.96	0.25	0.25
This work	0.77	0.16	1.02

(dimensionless function of temperature at a salinity of 35 pss; *Wanninkhof* [2014]), u_{10} is the 10 m height wind speed (m s^{-1}), and C_{eq} and C_w are the oxygen solubility and concentration in seawater (mol m^{-3}). P_a, P_b, and P_w are the partial pressures (in pascals) of oxygen in air bubbles (see *Stanley et al.* [2009] and equations (5) and (6)) and seawater. The α is the Bunsen solubility coefficient for oxygen (dimensionless), D is the diffusivity coefficient for oxygen gas (m^2 s^{-1}), and R is the gas constant (8.31 m^3 Pa mol^{-1} K^{-1}). D_o is a normalization factor to simplify units (m^2 s^{-1}). The constants, 9.1×10^{-11} s^2 m^{-2} and 2.3×10^{-3} in equations (5) and (6) are the tuned results from *Stanley et al.* [2009].

An unconstrained nonlinear optimization approach was used to tune the gas flux model. The sum of the squared differences between the nitrate- and oxygen-derived NCP seasonal cycles was minimized by adjusting the tunable parameters in our gas flux model (G_{EX}, G_C, and G_P), which weight the importance of the three flux terms in the model parameterization. After optimization the average ANCP estimate for oxygen was 1.5 mol C m^{-2} yr^{-1}, and the seasonal pattern was very similar to the nitrate-based estimate. The close agreement of the ANCP with the nitrate estimate results because the tuning process forces the oxygen-based rate to approach that of nitrate.

Table 3 compares the tuning coefficients from this work and those from *Nicholson et al.* [2012] with the values determined in *Stanley et al.* [2009]. The optimization scheme in this work reduces the importance of diffusive gas exchange and the gas flux from completely dissolving bubbles by 23% and 84%, respectively, but leaves the partially dissolving bubble flux approximation unchanged. In contrast the *Nicholson et al.* [2012] leaves the diffusive flux unchanged but reduces both the partially and completely dissolving bubble fluxes by 75%. All three approaches yield very different model tunings, though both this work and that of *Nicholson et al.* [2012] dramatically decrease the importance of the completely dissolving bubble flux (G_C).

The bubble flux results from a spectrum in bubble sizes. Approaches with completely and partially collapsed bubbles are effectively modeling two end-member types: large, partially dissolving, and small, completely dissolving bubbles. *Stanley et al.* [2009] optimized their model for maximum wind speeds of 12 m s^{-1}, but winter winds speeds at OSP can exceed 20 m s^{-1} (Figure 3a). The cubic dependency of the bubble gas flux upon wind speed would dramatically increase the importance of bubble exchange at OSP, relative to subtropical conditions studied by *Stanley et al.* [2009] or *Nicholson et al.* [2012], which provides a more robust environment in which the relative importance of bubble transport could be determined.

A similar tuning approach was used to optimize the three gas flux terms in equation (4) for the *Liang et al.* [2013] gas exchange model with one difference. Dimensionless multipliers were still used to tune the bubble fluxes, F_C and F_P [*Liang et al.*, 2013, equations (14) and (15)]. However, the diffusive exchange was optimized by tuning an adjustable parameter, A, in the transfer velocity formulation, K_s [*Liang et al.*, 2013, equation (9)]

$$K_S = \frac{u_*}{r_{wt}} \tag{8}$$

$$r_{wt} = \left(\frac{\rho_w}{\rho_a}\right)^{\frac{1}{2}} \left[\left(\frac{13.3}{A}\right) S_{cw}^{\frac{1}{2}} + k^{-1} \ln(z_w/\delta_w)\right] \tag{9}$$

where u_* is the friction velocity and r_{wt} is the waterside resistance to transfer due to molecular turbulent processes. The ρ_w and ρ_a are the density of air and water, S_{cw} is the Schmidt number for oxygen in water, z_w is the depth of the reference measurement, δ_w is the molecular sublayer thickness, and k is a constant equal to 0.4. Details about equation (9) can be found in *Fairall et al.* [2011].

In principal, A should be the same value for all gases, but the value was determined using carbon dioxide and dimethyl sulfide and not oxygen, a less soluble gas. After optimization A was reduced from 1.6 to 1.17, the partially dissolving bubble flux was reduced by 38%, and the completely dissolving bubble flux remained unchanged (Table 4). A smaller A value increases r_{wt} which decreases the transfer velocity and thus the diffusional gas exchange. After optimization the average ANCP was 1.5 mol C m^{-2} yr^{-1} (95% CI [0.7, 2.3]), the annual NCP cycle was similar to the nitrate-based NCP cycle, and the vertical ANCP profile (Figure 5c) for

Table 4. *Liang et al.* [2013] Model Tuning Coefficients

Reference	A	G_C	G_P
Liang et al. [2013]	1.6	1	1
This work	1.17	0.97	0.62

the upper 80 m was almost identical to the nitrate-based ANCP profile. The differences in optimizations and the pretuning ANCP estimates reinforce the point that ANCP estimates are very sensitive to the gas flux model used and the two end-member bubble flux parameterization may not adequately capture the bubble flux from the spectrum of bubble sizes.

To better understand the importance of each term in the gas exchange model, the average annual cycle for each model term is plotted as a rate and as fraction of the absolute magnitude of the total gas transport in Figure 9. These results are derived from the optimized *Liang et al.*, [2013] gas exchange model. From October through April the surface ocean absorbs oxygen and the partially and completely dissolving bubble fluxes dominate gas exchange. During this period 90% of the oxygen gas flux is due to bubble injection of gases, roughly 50% being driven by completely dissolving bubbles and 40% of the flux from partially dissolving bubbles (F_C and F_P). From May through September the ocean outgases oxygen and the completely dissolving bubble flux opposes the diffusional and partially dissolving bubble fluxes. During this period, diffusional gas exchange (F_{EX}) is responsible for about 75% of the gas flux and the partially dissolving bubble flux enhances outgassing and is responsible for another 10% to 15% of the total flux. Figure 9b shows that net productivity can be responsible for as much as 30% to 40% of the oxygen flux leaving the ocean in summer.

In addition to the choice of gas exchange model, oxygen-based NCP estimates are sensitive to the accuracy of oxygen measurements, especially when surface water oxygen concentrations are close to saturation. To emphasize this point, the oxygen-based NCP was recomputed using the *Liang et al.* [2013] gas exchange model, only the float oxygen concentrations were increased and decreased by 1% for all float data. Figure 7b shows oxygen-based NCP estimates for calibrated, calibrated plus 1%, and calibrated minus 1% float oxygen data sets. The general shape of the seasonal NCP cycle does not change significantly, but there are large changes in the ANCP value. ANCP for the calibrated data was 2.4 mol C m^{-2} yr^{-1}. When oxygen concentrations were increased by 1%, ANCP increased to 5.6 mol C m^{-2} yr^{-1}, and when they were lowered by 1%, ANCP became negative at −0.8 mol C m^{-2} yr^{-1}. A 2% overall change in oxygen concentration can shift ANCP estimates by approximately 6 mol C m^{-2} yr^{-1} in the northeast Pacific near OSP. A 0.5% uncertainty in oxygen calibration amounts to a 50% uncertainty in ANCP.

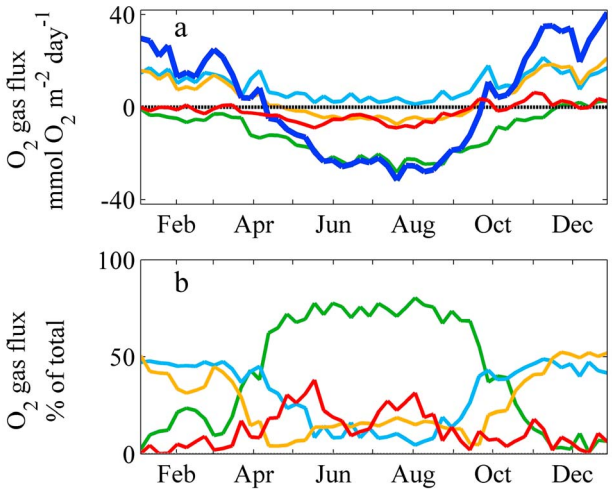

Figure 9. (a) Average annual oxygen flux across the air sea boundary using the optimized gas exchange model from *Liang et al.* [2013]: net (heavy blue), diffusive flux (green), completely dissolving bubble flux (light blue), partially dissolving bubble flux (orange), and oxygen flux due to biology (red). A positive flux is into the ocean. (b) The same as Figure 9 a above but plotted as a percent of the total absolute magnitude.

5. Discussion

In the Alaska gyre waters near OSP, nitrate sensors on profiling floats can offer a robust means to estimate NCP. A simple one-dimensional model appears to adequately capture the major physical processes (Figure 4). Nitrate is rarely depleted from the surface waters, the horizontal flow and nutrient gradients are weak [*Chelton et al.*, 2007], and nitrogen fixation is not considered an important source of nitrogen to the Gulf of Alaska surface waters [*Deutsch et al.*, 2007]. Therefore, the main source of nutrients at the surface is from below the halocline, and the only way to remove nitrate from the water is through net production of organic matter that is subsequently exported. Our 35 m integration depth is above the halocline. When ANCP is determined by integrating down to 80 m, the value drops from 1.5 to 1.2 mol C m^{-2} yr^{-1}. About 25% of the

Table 5. ANCP Estimates Near OSP[a]

Region	ANCP	Reference	Comments
OSP	1.5 (0.4)	*Wong et al.* [2002a]	NO_3^-, Line P, 1988–1998
Alaska Gyre	2.2	*Wong et al.* [2002b]	NO_3^-,1995–1996, Skaugran cruises
Subarctic Pacific	1.9	*Wong et al.* [2002b]	NO_3^-,1995–1996, Skaugran cruises
OSP	1.6 (0.6)	*Peña and Varela* [2007]	NO_3^-, Line P, 1969–2005
OSP	2.5	*Emerson and Stump* [2010]	N_2 and O_2 + model, 2007–2008
OSP	2.0	*Charette et al.* [1999]	POC, ^{234}Th + model, 1996–1997
OSP	0.7 (0.5)	*Bushinsky and Emerson* [2015]	O_2 + model, floats, June 2012 to June 2013
OSP	2 (1)	*Fassbender et al.* [2016]	Dissolved inorganic carbon and alkalinity + model, OSP, 2007–2014
OSP	1.5 (0.6)	This work	NO_3^- + model, floats, 2009–2014 (35 m integration depth)
OSP	1.5 (0.7)	This work	O_2 + optimized model, floats, 2009-2014 (35m integration depth)
OSP	1.2 (1.6)	This work	NO_3^- + optimized model, floats, 2009–2014 (80 m integration depth)
OSP	1.2 (1.6)	This work	O_2 + model, floats, 2009–2014 (80 m integration depth)

[a]Rate units in mol C m^{-2} yr^{-1} (±1 standard deviation). Our oxygen-based rate were computed using the *Liang et al.* [2013] gas exchange model optimized for OSP.

ANCP produced above 35 m is remineralized between this depth and the 80 m, possibly through nitrification. In contrast to nitrate-based estimates for NCP, where biology dominates nitrate removal from the mixed layer, the biological oxygen flux is relatively small and must be separated from a much larger physical flux, as oxygen is constantly moving in or out of the ocean as the air and water phases try to equilibrate due to changes in temperature, wind speed, and biology. The ANCP rates determined from oxygen are subject to larger uncertainties due to the gas exchange model and calibration of the oxygen sensors.

The average ANCP rates derived from profiling float nitrate and oxygen data are compared to several other estimates near OSP in Table 5. Estimates based on the seasonal depletion of nitrate [*Wong et al*., 2002a, 2002b; *Peña and Varela*, 2007] integrated down to 35 m as well as an approximation using 234^{Th} [*Charette et al*., 1999] and an estimate based on a dissolved inorganic carbon budget all lie within 1 standard deviation of the average profiling float estimates. *Emerson and Stump* [2010] calculate ANCP at 2.5 mol C m^{-2} yr^{-1} based on oxygen measurements, which is a little over 50% greater than the nitrate-derived estimate in this study. A 0.5% uncertainty in the oxygen measurements could easily account for this discrepancy. In addition, *Emerson and Stump* [2010] use the original *Stanley et al.* [2009] model (not optimized for OSP) with a different transfer velocity approximation. These differences could also be responsible for the difference between the two estimates. *Bushinsky and Emerson* [2015] determine a much lower estimate of 0.7 mol C m^{-2} yr^{-1} for the period June 2012 to June 2013 which is reasonably consistent with our estimates in this period, particularly the low ANCP in 2013 (Table 2).

5.1. Fate of ANCP

The vertical profiles of ANCP rates determined using nitrate and oxygen concentrations in conjunction with Redfieldian stoichiometry were qualitatively similar and of the same magnitude above 80 m (Figure 5c) once the gas flux model was optimized. Before optimization the oxygen-based ANCP rates diverged below 35 m to some extent, and this has been partially attributed to a modestly slow response of the oxygen sensor and partially to the gas exchange model not capturing all the exchange processes. This is not an issue with the nitrate sensor, which has a response time typically less than 1 s [*Johnson et al*., 2013]. The integral of the nitrate-based ANCP in the depth range from 35 to 80 m is -0.5 mol C m^{-2} yr^{-1}. This suggests that about 30% of the ANCP produced above 35 m is oxidized in this zone and the rest is exported below the halocline. This consumption rate likely continues with depth. However, the rates are low enough that they are difficult to detect with nitrate sensors.

5.2. Seasonality of NCP

Recently, there has been renewed interest as to what mechanisms initiate bloom conditions. This debate revolves around the interactions between mixing, light, and grazing, with the presumption that systems are not nutrient limited in late winter/early spring [*Behrenfeld*, 2010; *Boss and Behrenfeld*, 2010; *Taylor and Ferrari*, 2011]. Most of the discussion has focused on the North Atlantic. Mixed layer depths in the North Pacific are generally much shallower than in the North Atlantic, due to the strong halocline. Thus, the behavior in the North Pacific serves as an interesting counterpoint to observations in the North Atlantic.

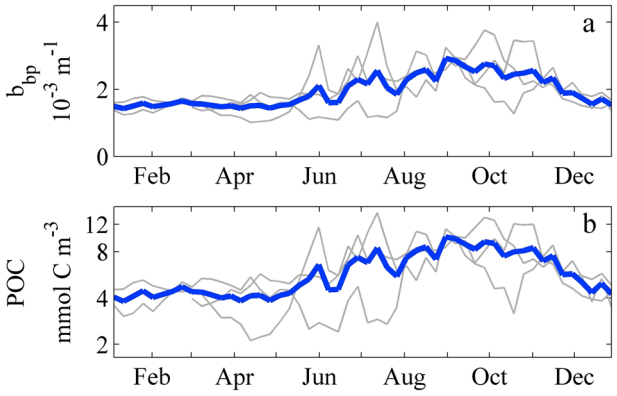

Figure 10. Average annual cycle over the top 35 m using optical backscatter data from floats 6400 and 7601 for the following: (a) the particulate backscattering coefficient, (b) Particulate organic carbon (POC) derived from the regression in *Graff et al.* [2015]: POC = ($b_{bp} \times 48{,}811 - 24$)/12 (note the log scale). Average of all years is in blue while individual years are in grey.

The seasonal NCP cycle shows that net production of organic matter starts in the beginning of February, almost 3 months before there is significant shoaling of the mixed layer depth (Figures 7a and 7c). The mixed layer represents the recent history of the maximum extent of mixing, but it may not be representative of the actively mixed layer in the surface ocean [*Brainerd and Gregg*, 1995; *Taylor and Ferrari*, 2011; *Franks*, 2014]. Active mixing at OSP can be assessed to some extent by comparing the 5 day average model mixing depth (depth at which the model homogenizes the mixed layer in each time step) to the mixed layer depth where density is 0.1 kg m^{-3} greater than surface value. The model mixing depth in Figure 7d is always shallower than the mixed layer depth displayed in Figure 8c, and model mixing only penetrates to a maximum of 75 m. Although the mixed layer does not begin to shoal until late April or the beginning of May, the active mixing depth begins shoaling at a date much closer to the onset of positive NCP, near the beginning of March.

These data imply that as active mixing begins to weaken in mid-winter and available light increases, while the mixed layer is still deep, net phytoplankton growth exceeds net respiratory losses and NCP in the actively mixed layer becomes positive. Such behavior in the North Atlantic is attributed to deep mixing and decoupling of phytoplankton growth rates from grazing rates [*Behrenfeld*, 2010]. Winter mixed layer depths and, presumably, mixing depths, can reach several hundred meters or more in the North Atlantic. At OSP the much shallower mixing and mixed layer depths would be much less effective at diluting zooplankton stocks and therefore less effective at reducing zooplankton grazing rates and decoupling the balance between phytoplankton and grazers [*Behrenfeld*, 2010]. POC values estimated from backscattering begin to increase in early February, at nearly the same time that NCP rates in the upper 35 m become positive (Figure 10b). These derived winter values of POC are high relative to the North Atlantic [*Behrenfeld*, 2010]. On average, the winter standing stock of POC is ~4 mmol C m^{-3} in the top 35 m, and it only doubles to ~ 7 mmol C m^{-3} in September (Figure 10b).

The accumulation of POC corresponds to an NCP of only 0.2 mol C m^{-2} yr^{-1}, nearly tenfold less than the NCP derived from changes in oxygen or nitrate concentrations. The POC produced by the NCP must be rapidly exported below the mixed layer. Grazing and remineralization within the upper 35 m would be less important because such a process would replenish nitrate and consume oxygen, reducing the estimated ANCP derived from chemical properties. Regardless of the process, the phytoplankton population appears to be under strong grazing control even in winter, consistent with prior understanding [*Boyd et al.*, 1995].

It is also possible that dissolved organic carbon (DOC) could build up in the summer surface waters coincident with positive NCP. DOC data from *Wong et al.* [2002a] suggest a maximum spring/summer increase of about 15 μM. This corresponds to ~0.9 μM potential decrease in nitrate assuming a C:N ratio of 1:16. This is about 12% of the annual nitrate drawdown in the surface waters or 12% of ANCP. If this surface produced that DON is advected to depth when the summer thermocline breaks down and then oxidized throughout the water column, this would show up as negative NCP at depth. This may be part of the negative nitrate-based ANCP signal seen between 45 and 100 m in Figures 5a or 5b (red line).

As the season progresses, the seasonal cycle of NCP exhibits two distinct peaks in NCP, one at the end of May and another at the beginning of August with a local rate minimum in between. These maxima correspond to maxima in the climatological rate of primary production measured by the ^{14}C method [*Boyd and Harrison*, 1999]. The local minimum in NCP corresponds to the annual peak in mesozooplankton biomass (>350 μm) toward the end of June [*Timothy et al.*, 2013, Figure 2j]. This period also coincides with high-incident solar

radiation and a relatively shallow mixing depth suggesting that phytoplankton growth rates should be high. Once the shoaling slows, perhaps the relatively stable physical environment allows the mesozooplankton growth to become more tightly coupled to phytoplankton growth, and very little net organic carbon is produced.

One of the most interesting questions that arise from the NCP data is what causes the termination of positive NCP each year? At the end of summer NCP begins to slow in concert with the erosion of the shallow mixing or mixed layer around August (Figure 7). *Timothy et al.* [2013] also compiled data that showed the primary production rates dramatically decrease around the same time of year that we observe NCP declines. The switch from positive to negative NCP in the mean rate curve occurs in September, when the actively mixed layer is only 25 m, well before deep mixing occurs. This is about the same depth when NCP is at a maximum at the end of May and much shallower than the 65 m depth of the actively mixed layer when NCP first becomes positive in March (Figure 7). Light levels would also be higher in September compared to March, when positive NCP begins. The physical environment is still quite suitable for phytoplankton growth.

What then is shifting the balance between primary production and respiratory losses? At the time of the NCP decrease, there is almost always nitrate present in the surface water. The standing stock of POC is at a maximum in September (Figure 10b). The mesozooplankton biomass curve shown in *Timothy et al.* [2013] peaks in June, and by September the zooplankton biomass is about one third of the maximum. Grazing and the subsequent remineralization of the phytoplankton carbon seem unlikely to produce the rapid decline in NCP. The waters near OSP are recognized to be iron limited [*Martin and Fitzwater*, 1988; *Boyd et al.*, 2004]. Possibly, the NCP decrease is the result of the onset of severe iron limitation late in the summer.

5.3. Float Constraints on Gas Exchange

Kihm and Körtzinger [2010] first demonstrated the potential application of profiling float oxygen data to better define gas exchange. Their calibrated data set from the Labrador Sea suggests that a cubic relationship to wind speed best defines the gas transfer velocity. They could not evaluate the influence of biological production because they had only oxygen as a tracer. Our work suggests that the use of profiling float data to understand gas exchange can be extended even further when multiple tracers are used. However, the optimization of oxygen gas exchange rates is dependent on the assumption that oxygen and nitrate cycling can be related by the Redfield ratio, which has some variability. As pH sensors are added to profiling floats, the seasonal cycle of dissolved inorganic carbon (DIC) can also be determined. The ratio of DIC to oxygen has much less flexibility than that of oxygen to nitrate does, and DIC has a different gas exchange behavior than oxygen does. The use of floats with pH, nitrate, and oxygen sensors would surely allow the uncertainties in gas exchange models and the relative ratios of elemental cycles to be more clearly defined.

Acknowledgments
This work was funded by NSF grant 0825348, National Ocean Partnership Program grant N00014 09 10052, and NOAA grant NA17RJ1232, part 2 to the University of Washington, and the David and Lucile Packard Foundation. This manuscript relied on data that were made freely available by NCEP, ERD, FNMOC, the Line P program, WOA, and the Monterey Bay Aquarium Research Institute (MBARI). Without these data sets, this work would not be possible. All Matlab scripts, input files, and output files used in this manuscript are available from the authors upon request (jplant@mbari.org). The data are archived at MBARI. This work was also made possible by everyone in the Chemical Sensor Program at MBARI and was greatly improved by the comments and suggestions supplied by two anonymous reviewers.

References

Amante, C., and B. W. Eakins (2009), ETOPO1 1 Arc-Minute Global Relief Model: Procedures, Data Sources and Analysis, NOAA Technical Memorandum NESDIS NGDC-24, National Geophysical Data Center, NOAA, doi:10.7289/V5C8276M.

Anderson, L. A. (1995), On the hydrogen and oxygen content of marine phytoplankton, *Deep Sea Res., Part I*, *42*(9), 1675–1680, doi:10.1016/0967-0637(95)00072-E.

Archer, D., S. Emerson, T. Powell, and C. S. Wong (1993), Numerical hindcasting of sea surface pCO_2 at weather station papa, *Prog. Oceanogr.*, *32*, 319–351, doi:10.1016/0079-6611(93)90019-A.

Babu, K. N., R. Sharma, N. Agarwal, and V. K. Agarwal (2004), Study of the mixed layer depth variations within the north Indian Ocean using a 1-D model, *J. Geophys. Res.*, *109*, C08016, doi:10.1029/2003JC002024.

Behrenfeld, M. J. (2010), Abandoning Sverdrup's critical depth hypothesis on phytoplankton blooms, *Ecology*, *91*(4), 977–989, doi:10.1890/09-1207.1.

Bittig, H. C., and A. Körtzinger (2015), Tackling oxygen optode drift: Near-surface and in-air oxygen optode measurements on a float provide an accurate in-situ reference, *J. Atmos. Oceanic Technol.*, doi:10.1175/JTECH-D-14-00162.1.

Bittig, H., B. Fiedler, R. Scholz, G. Krahmann, and A. Körtzinger (2014), Time response of oxygen optodes on profiling platforms and its dependence on flow speed and temperature, *Limnol. Oceanogr. Methods*, *12*, 617–636, doi:10.4319/lom.2014.12.617.

Bond, N. A., M. F. Cronin, H. Freeland, and N. Mantua (2015), Causes and impacts of the 2014 warm anomaly in the NE Pacific, *Geophys. Res. Lett.*, *42*, 3414–3420, doi:10.1002/2015GL063306.

Boss, E., and M. Behrenfeld (2010), In situ evaluation of the initiation of the North Atlantic phytoplankton bloom, *Geophys. Res. Lett.*, *37*, L18603, doi:10.1029/2010GL044174.

Boss, E., and W. S. Pegau (2001), Relationship of light scattering at an angle in the backward direction to the backscattering coefficient, *Appl. Opt.*, *40*(30), 5503–5507, doi:10.1364/AO.40.005503.

Boyd, P. W., and P. J. Harrison (1999), Phytoplankton dynamics in the NE subarctic Pacific, *Deep Sea Res., Part II*, *46*, 2405–2432, doi:10.1016/S0967-0645(99)00069-7.

Boyd, P. W., S. Strom, F. A. Whitney, S. Doherty, M. E. Wen, P. J. Harrison, and D. E. Varela (1995), The NE subarctic Pacific in winter: I. Biological standing stocks, *Mar. Ecol. Prog. Ser.*, *128*(1), 11–24, doi:10.3354/meps128011.

Boyd, P. W., D. L. Muggli, D. E. Varela, R. H. Goldblatt, R. Chretien, K. J. Orians, and P. J. Harrison (1996), In vitro iron enrichment experiments in the NE subarctic Pacific, *Mar. Ecol. Prog. Ser.*, *136*, 179–193, doi:10.3354/meps136179.

Boyd, P. W., et al. (2004), The decline and fate of an iron-induced subarctic phytoplankton bloom, *Nature*, *428*(6982), 549–553, doi:10.1038/nature02437.

Brainerd, K. E., and M. C. Gregg (1995), Surface mixed and mixing layer depths, *Deep Sea Res., Part I*, *42*(9), 1521–1543, doi:10.1016/0967-0637(95)00068-H.

Broecker, W. S., and T. H. Peng (1974), Gas exchange rates between air and sea, *Tellus*, *26*, 21–35, doi:10.1111/j.2153-3490.1974.tb01948.x.

Bushinsky, S. M., and S. Emerson (2015), Marine biological production from in situ oxygen measurements on a profiling float in the subarctic Pacific Ocean, *Global Biogeochem. Cycles*, *29*, 2050–2060, doi:10.1002/2015GB005251.

Charette, M. A., S. B. Moran, and J. K. Bishop (1999), ^{234}Th as a tracer of particulate organic carbon export in the subarctic northeast Pacific Ocean, *Deep Sea Res., Part II*, *46*(11), 2833–2861, doi:10.1016/S0967-0645(99)00085-5.

Chelton, D. M., G. Schlax, R. M. Samelson, and R. A. de Szoeke (2007), Global observations of large oceanic eddies, *Geophys. Res. Lett.*, *34*, L15606, doi:10.1029/2007GL030812.

Deutsch, C., J. L. Sarmiento, D. M. Sigman, N. Gruber, and J. P. Dunne (2007), Spatial coupling of nitrogen inputs and losses in the ocean, *Nature*, *445*, 163–167, doi:10.1038/nature05392.

D'Ortenzio, F., et al. (2014), Observing mixed layer depth, nitrate and chlorophyll concentrations in the northwestern Mediterranean: A combined satellite and NO3 profiling floats experiment, *Geophys. Res. Lett.*, *41*, 6443–6451, doi:10.1002/2014GL061020.

Emerson, S., and C. Stump (2010), Net biological oxygen production in the ocean - II: Remote in situ measurements of O_2 and N_2 in subarctic pacific surface waters, *Deep Sea Res., Part I*, *57*(10), 1255–1265, doi:10.1016/j.dsr.2010.06.001.

Emerson, S., P. Quay, C. Stump, D. Wilbur, and M. Knox (1991), O2, Ar, N2, and 222Rn in surface waters of the subarctic ocean: Net biological O2 production, *Global Biogeochem. Cycles*, *5*(1), 49–69, doi:10.1029/90GB02656.

Fairall, C. W., M. Yang, L. Bariteau, J. B. Edson, D. Helmig, W. McGillis, S. Pezoa, J. E. Hare, B. Huebert, and B. Blomquist (2011), Implementation of the Coupled Ocean-Atmosphere Response Experiment flux algorithm with CO2, dimethyl sulfide, and O3, *J. Geophys. Res.*, *116*, C00F09, doi:10.1029/2010JC006884.

Falkowski, P., et al. (2000), The global carbon cycle: A test of our knowledge of earth as a system, *Science*, *290*, 291, doi:10.1126/science.290.5490.291.

Fassbender, A. J., C. L. Sabine, and M. F. Cronin (2016), Net community production and calcification from 7 years of NOAA Station Papa Mooring measurements, *Global Biogeochem. Cycles*, *30*, 250–267, doi:10.1002/2015GB005205.

Franks, P. J. (2014), Has Sverdrup's critical depth hypothesis been tested? Mixed layers vs. turbulent layers, *ICES J. Mar. Sci.*, doi:10.1093/icesjms/fsu175.

Freeland, H. (2007), A short history of Ocean Station Papa and Line P, *Prog. Oceanogr.*, *75*, 120–125, doi:10.1016/j.pocean.2007.08.005.

Freeland, H. J. (2013), Vertical velocity estimates in the North Pacific using Argo floats, *Deep Sea Res., Part II*, *85*, 75–80, doi:10.1016/j.dsr2.2012.07.019.

Garcia, H. E., R. A. Locarnini, T. P. Boyer, J. I. Antonov, M. M. Zweng, O. K. Baranova, and D. R. Johnson (2010), *World Ocean Atlas 2009, Volume 4: Nutrients (Phosphate, Nitrate, Silicate)*, *NOAA Atlas NESDIS 71*, edited by S. Levitus, 398 pp., U.S. Gov. Print. Off., Washington, D. C.

Glover, D. M., W. J. Jenkins, and S. C. Doney (2011), *Modeling Methods for Marine Science*, pp. 365–407, Cambridge Univ. Press, Cambridge, U. K.

Graff, J. R., T. K. Westberry, A. J. Milligan, M. B. Brown, G. Dall'Olmo, V. van Dongen-Vogels, K. M. Reifel, and M. J. Behrenfeld (2015), Analytical phytoplankton carbon measurements spanning diverse ecosystems, *Deep Sea Res., Part I*, *102*, 16–25, doi:10.1016/j.dsr.2015.04.006.

Hamme, R. C., and S. R. Emerson (2002), Mechanisms controlling the global oceanic distribution of the inert gases argon, nitrogen and neon, *Geophys. Res. Lett.*, *29*(23), 2120, doi:10.1029/2002GL015273.

Harrison, P. J., F. A. Whitney, A. Tsuda, H. Saito, and K. Tadokoro (2004), Nutrient and plankton dynamics in the NE and NW gyres of the subarctic Pacific Ocean, *J. Oceanogr.*, *60*(1), 93–117, doi:10.1023/B:JOCE.0000038321.57391.2a.

Ho, D. T., R. Wanninkhof, P. Schlosser, D. S. Ullman, D. Hebert, and K. F. Sullivan (2011), Toward a universal relationship between wind speed and gas exchange: Gas transfer velocities measured with 3He/SF6 during the Southern Ocean Gas Exchange Experiment, *J. Geophys. Res.*, *116*, C00F04, doi:10.1029/2010JC006854.

Johnson, K. S., W. M. Berelson, E. S. Boss, Z. Chase, H. Claustre, S. R. Emerson, N. Gruber, A. Kortzinger, M. J. Perry, and S. C. Riser (2009), Observing biogeochemical cycles at global scales with profiling floats and gliders prospects for a global array, *Oceanography*, *22*(3), 216–225, doi:10.5670/oceanog.2009.81.

Johnson, K. S., S. C. Riser, and D. M. Karl (2010), Nitrate supply from deep to near-surface waters of the North Pacific subtropical gyre, *Nature*, *465*(7301), 1062–1065, doi:10.1038/nature09170.

Johnson, K. S., L. Coletti, H. Jannasch, C. Sakamoto, D. Swift, and S. Riser (2013), Long-term nitrate measurements in the ocean using the In Situ Ultraviolet Spectrophotometer: Sensor integration into the Apex profiling float, *J. Atmos. Oceanic Technol.*, doi:10.1175/JTECH-D-12-00221.1.

Johnson, K., J. Plant, S. Riser, and D. Gilbert (2015), Air oxygen calibration of oxygen optodes on a profiling float array, *J. Atmos. Oceanic Technol.*, *32*, 2160–2172, doi:10.1175/JTECH-D-15-0101.1.

Kalnay, E., et al. (1996), The NCEP/NCAR 40-year reanalysis project, *Bull. Am. Meteorol. Soc.*, *77*, 437–470, doi:10.1175/1520-0477(1996)077<0437:TNYRP>2.0.CO;2.

Kihm, C., and A. Körtzinger (2010), Air-sea gas transfer velocity for oxygen derived from float data, *J. Geophys. Res.*, *115*, C12003, doi:10.1029/2009JC006077.

Körtzinger, A., J. Schimanski, U. Send, and D. Wallace (2004), The ocean takes a deep breath, *Science*, *306*(5700), 1337–1337, doi:10.1126/science.1102557.

Large, W. G. (1996), An observational and numerical investigation of the climatological heat and salt balances at OWS Papa, *J. Clim.*, *9*(8), 1856–1876, doi:10.1175/1520-0442(1996)009<1856:AOANIO>2.0.CO;2.

Laws, E. A. (1991), Photosynthetic quotients, new production and net community production in the open ocean, *Deep Sea Res. Part. A.*, *38*(1), 143–167, doi:10.1016/0198-0149(91)90059-O.

Liang, J. H., C. Deutsch, J. C. McWilliams, B. Baschek, P. P. Sullivan, and D. Chiba (2013), Parameterizing bubble-mediated air-sea gas exchange and its effect on ocean ventilation, *Global Biogeochem. Cycles*, *27*, 894–905, doi:10.1002/gbc.20080.

Luz, B., and E. Barkan (2000), Assessment of oceanic productivity with the triple-isotope composition of dissolved oxygen, *Science*, *228*, 2028–2031, doi:10.1126/science.288.5473.2028.

Maldonado, M. T., P. W. Boyd, P. J. Harrison, and N. M. Price (1999), Co-limitation of phytoplankton growth by light and Fe during winter in the NE subarctic Pacific Ocean, *Deep Sea Res., Part II*, *46*(11), 2475–2485, doi:10.1016/S0967-0645(99)00072-7.

Martin, J. H., and S. E. Fitzwater (1988), Iron deficiency limits phytoplankton growth in the north-east Pacific subarctic, *Nature*, *331*, 341–343, doi:10.1038/331341a0.
Martz, T. M., M. D. DeGrandpre, P. G. Strutton, W. R. McGillis, and W. M. Drennan (2009), Sea surface pCO_2 and carbon export during the Labrador Sea spring-summer bloom: An in situ mass balance approach, *J. Geophys. Res.*, *114*, C09008, doi:10.1029/2008JC005060.
Matear, R. J., and C. S. Wong (1997), Estimation of vertical mixing in the upper ocean at Station P from chlorofluorocarbons, *J. Mar. Res.*, *55*(3), 507–521, doi:10.1357/0022240973224300.
Mathieu, T., and B. DeYoung (1995), Application of a mixed layer model to the inner Newfoundland shelf, *J. Geophys. Res.*, *110*(C1), 921–936, doi:10.1029/94JC01435.
McGillis, W. R., J. B. Edson, J. E. Hare, and C. W. Fairall (2001), Direct covariance air-sea CO2 fluxes, *J. Geophys. Res.*, *106*(C8), 16,729–16,745, doi:10.1029/2000JC000506.
Miller, C. B., B. W. Frost, P. A. Wheeler, M. R. Landry, N. Welschmeyer, and T. M. Powell (1991), Ecological dynamics in the Subarctic Pacific, a possibly iron-limited ecosystem, *Limnol. Oceanogr.*, *36*(8), 1600–1615, doi:10.4319/lo.1991.36.8.1600.
Nicholson, D. P., R. H. Stanley, E. Barkan, D. M. Karl, B. Luz, P. D. Quay, and S. C. Doney (2012), Evaluating triple oxygen isotope estimates of gross primary production at the Hawaii Ocean Time-series and Bermuda Atlantic Time-series Study sites, *J. Geophys. Res.*, *117*, C05012, doi:10.1029/2010JC006856.
Parekh, P., S. Dutkiewicz, M. J. Follows, and T. Ito (2006), Atmospheric carbon dioxide in a less dusty world, *Geophys. Res. Lett.*, *33*, L03610, doi:10.1029/2005GL025098.
Paulson, C. A., and J. J. Simpson (1977), Irradiance measurements in the upper ocean, *J. Phys. Oceanogr.*, *7*(6), 952–956, doi:10.1175/1520-0485(1977)007<0952:IMITUO>2.0.CO;2.
Peña, M. A., and D. E. Varela (2007), Seasonal and interannual variability in phytoplankton and nutrient dynamics along Line P in the NE subarctic Pacific, *Prog. Oceanogr.*, *75*, 200–222, doi:10.1016/j.pocean.2007.08.009.
Price, J. F., R. A. Weller, and R. Pinkel (1986), Diurnal Cycling: Observations and models of the upper ocean response to diurnal heating, cooling and wind mixing, *J. Geophys. Res.*, *91*, 8411–8427, doi:10.1029/JC091iC07p08411.
Prytherch, J., M. J. Yelland, R. W. Pascal, B. I. Moat, I. Skjelvan, and M. A. Srokosz (2010), Open ocean gas transfer velocity derived from long-term direct measurements of the CO2 flux, *Geophys. Res. Lett.*, *37*, L23607, doi:10.1029/2010GL045597.
Ren, L., and S. C. Riser (2009), Seasonal salt budget in the northeast Pacific Ocean, *J. Geophys. Res.*, *114*, C12004, doi:10.1029/2009JC005307.
Riser, S. C., and K. S. Johnson (2008), Net production of oxygen in the subtropical ocean, *Nature*, *451*(7176), 323–325, doi:10.1038/nature06441.
Sherry, N. D., P. W. Boyd, K. Sugimoto, and P. J. Harrison (1999), Seasonal and spatial patterns of heterotrophic bacterial production, respiration, and biomass in the subarctic NE Pacific, *Deep Sea Res., Part II*, *46*(11), 2557–2578, doi:10.1016/S0967-0645(99)00076-4.
Signorini, S. R., C. R. McClain, J. R. Christian, and C. S. Wong (2001), Seasonal and interannual variability of phytoplankton, nutrients, TCO_2, pCO_2 and O_2 in the eastern subarctic Pacific (ocean weather station Papa), *J. Geophys. Res.*, *106*, 31,197–31,215, doi:10.1029/2000JC000343.
Stanley, R. H. R., W. J. Jenkins, and S. C. Doney (2006), Quantifying seasonal air-sea gas exchange processes using noble gas time-series: A design experiment, *J. Mar. Res.*, *64*(2), 267–295, doi:10.1357/002224006777606452.
Stanley, R. H. R., W. J. Jenkins, D. E. Lott III, and S. C. Doney (2009), Noble gas constraints on air-sea gas exchange and bubble fluxes, *J. Geophys. Res.*, *114*, C11020, doi:10.1029/2009JC005396.
Sunda, W. G., and S. A. Huntsman (1997), Interrelated influence of iron, light and cell size on marine phytoplankton growth, *Nature*, *390*, 389–392, doi:10.1038/37093.
Takeshita, Y., T. R. Martz, K. S. Johnson, J. N. Plant, D. Gilbert, S. C. Riser, C. Neill, and B. Tilbrook (2013), A climatology-based quality control procedure for profiling float oxygen data, *J. Geophys. Res. Oceans*, *118*, 5640–5650, doi:10.1002/jgrc.20399.
Taylor, J. R., and R. Ferrari (2011), Shutdown of turbulent convection as a new criterion for the onset of spring phytoplankton blooms, *Limnol. Oceanogr.*, *56*(6), 2293–2307, doi:10.4319/lo.2011.56.6.2293.
Tengberg, A., et al. (2006), Evaluation of a lifetime-based optode to measure oxygen in aquatic systems, *Limnol. Oceanogr. Methods*, *4*, 7–17, doi:10.4319/lom.2006.4.7.
Timothy, D. A., C. S. Wong, J. E. Barwell-Clarke, J. S. Page, L. A. White, and R. W. Macdonald (2013), Climatology of sediment flux and composition in the subarctic Northeast Pacific Ocean with biogeochemical implications, *Prog. Oceanogr.*, *116*, 95–129, doi:10.1016/j.pocean.2013.06.017.
Varela, D. E., and P. J. Harrison (1999), Seasonal variability in nitrogenous nutrition of phytoplankton assemblages in the northeastern subarctic Pacific Ocean, *Deep Sea Res., Part II*, *46*(11), 2505–2538, doi:10.1016/S0967-0645(99)00074-0.
Wanninkhof, R. (1992), Relationship between wind speed and gas exchange over the ocean, *J. Geophys. Res.*, *97*(25), 7373–7382, doi:10.1029/92JC00188.
Wanninkhof, R. (2014), Relationship between wind speed and gas exchange over the ocean revisited, *Limnol. Oceanogr. Methods*, *12*(6), 351–362, doi:10.4319/lom.2014.12.351.
Watson, A. J., and J. C. Orr (2003), Carbon Dioxide Fluxes in the Global Ocean, in *Ocean Biogeochemistry: The Role of the Ocean Carbon Cycle in Global Change*, *Global Change - The IGBP Ser.*, edited by M. J. R. Fasham, pp. 123–143, Springer, Berlin.
Whitney, F. A., and H. J. Freeland (1999), Variability in upper-ocean water properties in the NE Pacific Ocean, *Deep Sea Res., Part II*, *46*(11), 2351–2370, doi:10.1016/S0967-0645(99)00067-3.
Williams, P. J. L. (1993), On the definition of plankton production terms, *ICES Mar. Sci. Symp.*, *197*, 9–19.
Wong, C. S., F. A. Whitney, R. J. Matear, and K. Iseki (1998), Enhancement of new production in the northeast subarctic Pacific Ocean during negative North Pacific index events, *Limnol. Oceanogr.*, *43*(7), 1418–1426, doi:10.4319/lo.1998.43.7.1418.
Wong, C. S., N. A. D. Waser, F. A. Whitney, W. K. Johnson, and J. S. Page (2002a), Time-series study of the biogeochemistry of the North East subarctic Pacific: Reconciliation of the C org/N remineralization and uptake ratios with the Redfield ratios, *Deep Sea Res., Part II*, *49*(24), 5717–5738, doi:10.1016/S0967-0645(02)00211-4.
Wong, C. S., N. A. D. Waser, Y. Nojiri, F. A. Whitney, J. S. Page, and J. Zeng (2002b), Seasonal cycles of nutrients and dissolved inorganic carbon at high and mid latitudes in the North Pacific Ocean during the Skaugran cruises: Determination of new production and nutrient uptake ratios, *Deep Sea Res., Part II*, *49*(24), 5317–5338, doi:10.1016/S0967-0645(02)00193-5.
Woolf, D. K., and S. A. Thorpe (1991), Bubbles and the air-sea exchange of gases in near-saturation conditions, *J. Mar. Res.*, *49*, 435–466, doi:10.1357/002224091784995765.